Triplet-Tuning: A Novel Family of Non-Empirical Exchange–Correlation Functionals

Zhou Lin and Troy Van Voorhis*

Department of Chemistry, Massachusetts Institute of Technology, Cambridge, MA 02139

E-mail: tvan@mit.edu

Abstract

In the framework of density functional theory (DFT), the lowest triplet excited state, T_1, can be evaluated using multiple formulations, the most straightforward of which are unrestricted DFT (UDFT) and time-dependent DFT (TDDFT). Assuming the exact exchange–correlation (XC) functional is applied, UDFT and TDDFT provide identical energies for T_1 (E_T), which is also a constraint that we require our XC functionals to obey. However, this condition is not satisfied by most of the popular XC functionals, leading to inaccurate predictions of low-lying, spectroscopically and photochemically important excited states, such as T_1 and the lowest singlet excited state (S_1). Inspired by the optimal tuning strategy for frontier orbital energies [T. Stein, L. Kronik, and R. Baer, *J. Am. Chem. Soc.* **131**, 2818 (2009)], we proposed a novel and *non-empirical* prescription of constructing an XC functional in which the agreement between UDFT and TDDFT in E_T is strictly enforced. Referred to as "triplet tuning", our procedure allows us to formulate the XC functional on a case-by-case basis using the molecular structure as the exclusive input, without fitting to any experimental data. The first triplet tuned XC functional, TT-ωPBEh, is formulated as a long-range-corrected (LRC) hybrid of Perdew–Burke–Ernzerhof (PBE) and Hartree–Fock (HF) functionals [M. A. Rohrdanz, K. M. Martins, and J. M. Herbert, *J. Chem. Phys.* **130**, 054112 (2009)] and tested on four sets of large organic molecules. Compared to existing functionals, TT-ωPBEh manages to provide

more accurate predictions for key spectroscopic and photochemical observables, including but not limited to E_{T}, the optical band gap (E_{S}), the singlet–triplet gap (ΔE_{ST}), and the vertical ionization potential ($I_{\perp}$), as it adjusts the effective electron-hole interactions to arrive at the correct excitation energies. This promising triplet tuning scheme can be applied to a broad range of systems that were notorious in DFT for being extremely challenging.

1 Introduction

Due to its affordable computational cost, density functional theory (DFT) has become the main theoretical workhorse for large molecules where most wave function based approaches are infeasible.[1–4] DFT was originally established as a ground-state approach, while various excited-state extensions were also formulated to predict experimental observables. Representative excited-state methods include time-dependent DFT (TDDFT),[5] spin-flip DFT (SFDFT),[6] Δ self-consistent field (ΔSCF),[7] and restricted open-shell Kohn–Sham (ROKS).[8] Despite being formally exact, DFT has several fundamental issues which place a glass ceiling over its predictive power for excited states, especially for organic molecules with large π-conjugated structures or charge transfer characters. For example, the accuracy of a (semi-)empirical density functional heavily relies on the selection of parameters in its exchange–correlation (XC) component (E_{XC}). Optimal parameters are sensitive to the configurational features of species included in the fitting database. Also, the self-interaction error (SIE) and the locality problem can lead to unphysical density distributions in both short and long ranges for those difficult molecules.[9–17]

Within the recent decade, many methodological efforts have been reported to resolve above-mentioned issues. For instance, new DFT variants have been developed, such as self-interaction corrected DFT (SIC-DFT),[18] average density self-interaction correction (ADSIC),[19] constrained DFT (CDFT),[20] and constrained variational DFT (CV(∞)-DFT).[21] Without modifying the conventional DFT-based approaches, new XC functionals have also been constructed to approximate the exact density. Typical examples include $meta$-generalized gradient approximation ($meta$-GGA) that involves the second gradient of the density (TPSS,[22] SCAN,[23] M06-L,[24] and M06-2X,[25] *etc.*), and range-separation treatment that partially or fully reproduces the asymptotic density decay by implementing the Hartree–Fock (HF) exchange in the long range using an empirically determined range-separation parameter, ω (CAM-B3LYP,[26] CAM-QTP,[27] ωB97X-V,[28] ωB97M-V,[29] LRC-ωPBE,[30,31] and LRC-ωPBEh,[32,33] *etc.*).

More recently, several optimally tuned (OT) versions of range-separated XC functionals have been proposed and applied to large molecules, including OT-BNL,[34] OT-ωB97XD,[35] and OT-

ωPBEh,[36] *etc.* These functionals allow the users to optimize ω in a *non-empirical*, system-dependent fashion, and can be considered as a "black box" in which the molecular structure serves as the exclusive input. As an outstanding example, Kronik, Baer, and co-workers developed the most popular optimal tuning scheme[34,37,38] based on Iikura's idea of range separation[39] and Koopmans' theorem.[40] They enforce an agreement between the vertical ionization potential ($I_\perp$) and the negative eigenvalue for the highest occupied molecular orbital ($-\varepsilon^{(N)}_{\mathrm{HOMO}}$), which is satisfied by the exact XC functional. These optimally tuned functionals have successfully predicted diverse (pseudo-)one-electron properties such as the fundamental band gap, the photoelectron spectrum, and the charge transfer excitation energy. Also, they behave reasonably well for spectroscopic and photochemical properties like the optical band gap ($E_{\mathrm{S}} = E_{\mathrm{S}_1} - E_{\mathrm{S}_0}$), the phosphorescence energy ($E_{\mathrm{T}} = E_{\mathrm{T}_1} - E_{\mathrm{S}_0}$), and the singlet–triplet gap ($\Delta E_{\mathrm{ST}} = E_{\mathrm{S}_1} - E_{\mathrm{T}_1}$).[41–48] However, as these functionals are not explicitly tuned for low-lying energetics, their for accuracy these quantities is not expected to be comparable with (pseudo-)one-particle properties.

Motivated by reaching more accurate predictions of spectroscopically and photochemically important excited states, we proposed the novel triplet tuning scheme based on the lowest triplet excited state (T_1). Our idea borrows a page from the above-mentioned optimal tuning prescription,[34,37,38] in which we optimized the values of one or two selected parameters in a *non-empirical* manner by matching a particular energy level evaluated using two different approaches. Instead of equaling $I_\perp$ to $-\varepsilon^{(N)}_{\mathrm{HOMO}}$, we enforced the agreement in the lowest triplet excitation energy (E_{T}) between two excited-state DFT formulations, namely ΔSCF[7] and TDDFT.[5]

In the present study, we developed the first triplet tuned (TT) functional in this series, TT-ωPBEh, by imitating the formula of LRC-ωPBEh[30,31] and leaving two adjustable parameters: ω and the percentage of the HF exchange in the short range, C_{HF}. The methodological details will be provided in Sec. 2. In Sec. 3, the accuracy and stability of TT-ωPBEh will be analyzed using four groups of large organic molecules which possess rich spectroscopic and photochemical information and are notoriously difficult for theoretical investigations, even for low-lying excited states. As will be illustrated by Sec. 3, TT-ωPBEh provides the most excellent agreement with

experiments regarding E_{T}, E_{S}, and ΔE_{ST}, due to its accurate reproduction of the screening of the electron-hole interaction. Concerning $I_{\perp}$, we will show that the incorporation of triplet tuning will enhance the predictive power of the conventional optimal tuning prescription. The conclusion and the future work will be discussed in Sec. 4.

2 Theory

2.1 Triplet Excitation Energy

Constructed by Kohn and Sham (KS-DFT), the most popular version of DFT allows us to evaluate the energy and density based on molecular orbitals.[2,3] In this framework, there exists a universal, variational functional that provides the correct ground-state energy from the exact ground-state density. It is also straightforward to generalize the KS functional to one that gives the lowest state of a system with *any given symmetry* when constraining the density to the corresponding symmetry.[49] As a result, ground-state DFT is able to access an excited state that is the lowest state within a particular symmetry. The most common case of this has to do with the spin configuration. When the true ground state for a closed-shell molecule (like most organic molecules) is a spin-restricted singlet (S_0), the lowest state with $M_S = \pm 1$ must be a triplet (T_1). These closed-shell species can achieve T_1 by promoting one electron from HOMO to the lowest unoccupied molecular orbital (LUMO) and flipping its spin accordingly. S_0 and T_1 can be most easily resolved by doing a restricted DFT (RDFT) calculation with $M_S = 0$ in the former case and an UDFT calculation with $M_S = \pm 1$ in the latter.[50] Therefore, the triplet excitation energy, E_{T}, which corresponds to an experimental measure of E_{T_1}, can be evaluated following the ΔSCF scheme,

$$E_{\mathrm{T}}^{\Delta\mathrm{SCF}} = E_{\mathrm{T}_1}^{\mathrm{UDFT}} - E_{\mathrm{S}_0}^{\mathrm{RDFT}}. \tag{1}$$

Under the exact functional, Eq. (1) gives the true E_{T}. In an alternative strategy, T_1 can be treated as an excited state using linear-response TDDFT.[5,51] With the exact XC kernel TDDFT yields exact

energies for *all* excited states including T_1.[52] As such, E_T can also be obtained using

$$E_T^{TDDFT} = E_{T_1}^{TDDFT} - E_{S_0}^{RDFT}. \quad (2)$$

2.2 Triplet Tuning Protocol

Since RDFT, UDFT, and TDDFT are all formally exact approaches, Eqs. (1) and (2) would provide identical values of E_T assuming the exact XC functional and kernel are used,

$$E_T^{\Delta SCF} \equiv E_T^{TDDFT}. \quad (3)$$

However, we note that for an approximate functional, Eq. (3) does not necessarily hold, and the difference between $E_T^{\Delta SCF}$ and E_T^{TDDFT} strictly measures one aspect of the inaccuracy of the underlying functional. Eq. (3) is analogous to the Koopmans' theorem that the frontier orbital energies, $-\varepsilon_{HOMO}^{(N)}$ and $-\varepsilon_{LUMO}^{(N)}$, should match $I_\perp$ and the vertical electron affinity ($A_\perp$) respectively under the exact XC functional.[3,34,37,38,40,53] However, our case differs from the conventional optimal tuning by using an excited state as a target of interest rather than an ionized ground state.

Thus, learning from the optimal tuning approach,[34,37,38] our key concept is to tune the underlying functional on a molecule-by-molecule basis so that Eq. (3) is fulfilled as rigorously as possible. In practice, we minimized the following objective function,

$$J_{TT}^2 = \left(E_T^{\Delta SCF} - E_T^{TDDFT}\right)^2, \quad (4)$$

in order to obtain optimal parameters. We refer to this approach as "triplet tuning", which can be utilized to improve the performance of any XC functional. We should note that TT *does not introduce any empiricism* to the underlying functional, as the calculated $E_T^{\Delta SCF}$ and E_T^{TDDFT} are not matched to any experimental value – instead the parameters are optimized to achieve an internal consistency of $E_T^{\Delta SCF}$ and E_T^{TDDFT} that the exact functional is known to possess.

Similar to optimal tuning, our triplet tuning protocol can be partly justified based on the adi-

abatic connection:[54] the exact E_{XC} is related to the coupling-constant-average of the electron-electron interaction energy, for which the value at the low-coupling limit is just the exchange energy (E_{X}) and the stronger coupling is embodied in the correlation energy (E_{C}). The precise weight of weakly and strongly interacting systems in the integral depends on the system and the range of the interaction and must typically be determined semi-empirically.[30,32,55] The triplet tuning scheme offers the attractive possibility of performing the adiabatic connection in a *non-empirical* fashion, that is, minimizing J_{TT}^2 in Eq. (4) to define the optimal form of E_{XC}. In the present study, we focused on the tuning of E_{X} as its weight is significant heavier than E_{C} for most weakly interacting molecules of interest.

Bearing this in mind, we performed triple tuning on the basis of the range-separated hybrid formula of PBE and HF,[30–33,56] and named it as TT-ωPBEh. TT-ωPBEh was designed to predict the accurate density in both short and long ranges and to reproduce the correct electron-hole interactions in molecules. Its formula separates E_{X} into the short-range (SR) and long-range (LR) contributions,[39]

$$E_{\mathrm{XC}} = E_{\mathrm{X}}^{\mathrm{SR}} + E_{\mathrm{X}}^{\mathrm{LR}} + E_{\mathrm{C}}. \tag{5}$$

This can be accomplished by re-expressing the Coulomb operator, $1/r_{12}$, into[39,57]

$$\frac{1}{r_{12}} = \underbrace{\frac{1-\mathrm{erf}(\omega \mathrm{r}_{12})}{r_{12}}}_{\mathrm{SR}} + \underbrace{\frac{\mathrm{erf}(\omega \mathrm{r}_{12})}{r_{12}}}_{\mathrm{LR}}, \tag{6}$$

in which $r_{12} = |\vec{r}_1 - \vec{r}_2|$ is the interelectron distance, and "erf" represents the Gauss error function.[58] Eq. (6) introduces ω as the range-separation parameter, which is the reciprocal of the distance at which $E_{\mathrm{X}}^{\mathrm{SR}}$ transitions to $E_{\mathrm{X}}^{\mathrm{LR}}$.[39] As the non-local HF exchange exhibits the correct asymptotic behavior,[57] we selected

$$E_{\mathrm{X}}^{\mathrm{LR}} \equiv E_{\mathrm{X}}^{\mathrm{HF}}. \tag{7}$$

Meanwhile, $E_{\mathrm{X}}^{\mathrm{SR}}$ takes a hybrid form of HF and a selected (semi-)local DFT exchange functional in

order to balance the localization error from HF and delocalization error from this DFT functional:[59]

$$E_{\mathrm{X}}^{\mathrm{SR}} = C_{\mathrm{HF}} E_{\mathrm{X,HF}}^{\mathrm{SR}} + C_{\mathrm{DFT}} E_{\mathrm{X,DFT}}^{\mathrm{SR}}. \tag{8}$$

C_{HF} and C_{DFT} represent the fractions of the HF and DFT components in $E_{\mathrm{X}}^{\mathrm{SR}}$, and they are related to each other through the uniform electron gas (UEG) constraint,[1–4]

$$C_{\mathrm{HF}} + C_{\mathrm{DFT}} = 1. \tag{9}$$

Eqs. (8) and (9) suggest the second to-be-determined parameter, C_{HF}. In existing range-separated hybrid formulations, E_{C} and $E_{\mathrm{X,DFT}}^{\mathrm{SR}}$ can be selected among LDA,[2] GGA,[60–62] or $meta$-GGA[22–25] expressions based on the requirement of the system. In TT-ωPBEh one utilizes the Perdew–Burke–Ernzerhof (PBE) formulas for $E_{\mathrm{X,DFT}}^{\mathrm{SR}}$ and E_{C}.[63]

In the present study, we examined three variants of TT-ωPBEh, one with both parameters tuned (the original TT-ωPBEh), and two with a single tunable parameter, either ω (TT-ωPBEhω, similar to LRC-ωPBEh[33]) or C_{HF} (TT-ωPBEhC). Such a comparison enables us to validate the insufficiency of the single-parameters versions and the necessity of tuning both ω and C_{HF}.

2.3 One-Electron Property

As was discussed in Sec. 1, our triplet tuning scheme reproduces correct electron-hole interactions while the optimal tuning prescription of Kronik and Baer provides accurate one-electron properties.[34,37,38] Therefore a performance comparison between these two approaches is necessary. To realize this we also re-constructed the range-separated hybrid OT-ωPBEh functional as described in Eqs. (5)–(9). The objective function was established following Koopmans' theorem,[34,37,38,40]

$$J_{\mathrm{OT}}^2 = \left[I_\perp + \varepsilon_{\mathrm{HOMO}}^{(N)} \right]^2 + \left[A_\perp + \varepsilon_{\mathrm{HOMO}}^{(N+1)} \right]^2, \tag{10}$$

where $\varepsilon_{\mathrm{HOMO}}^{(N+1)}$ stands for the HOMO energy of the anionic species with an identical molecular structure to the neutral species and is a substitute of $\varepsilon_{\mathrm{LUMO}}^{(N)}$ due to the incorrect physical interpretation of virtual orbitals in the KS framework.[3,53] $I_\perp$ and $A_\perp$ are evaluated using ΔSCF,

$$I_\perp = E_{\mathrm{C}^+}^{\mathrm{UDFT}} - E_{\mathrm{S}_0}^{\mathrm{RDFT}}, \tag{11}$$

$$A_\perp = E_{\mathrm{S}_0}^{\mathrm{RDFT}} - E_{\mathrm{A}^-}^{\mathrm{UDFT}}, \tag{12}$$

where C^+ and A^- represent cationic and anionic species respectively.

In an attempt to take into account both one-electron properties and electron-hole interactions using the very same functional, we also combined the recipes of OT-ωPBEh and TT-ωPBEh to formulate another functional termed as mix-ωPBEh. Its objective function is consequently

$$J_{\mathrm{mix}}^2 = \frac{J_{\mathrm{TT}}^2 + J_{\mathrm{OT}}^2}{2}. \tag{13}$$

2.4 Molecular Test Sets

In order to evaluate the performance and applicability of TT-ωPBEh and mix-ωPBEh and compare their behaviors to OT-ωPBEh and existing functionals, we selected a total of 110 organic molecules, most of which posses semiconducting structures or charge transfer characters and reliable experimental measurements of E_{T}, E_{S}, ΔE_{ST}, and $I_\perp$. In spite of being closed-shell, these species are notorious as challenging cases for theoretical investigations. Molecules were divided into four test sets based on their structural features, excited-state properties, and real-life applications, including polycyclic aromatic hydrocarbons (PAH),[64–97] organic photovoltaics (OPV) materials,[43,64,70,72,75,83,98–173] thermally activated delayed fluorescence (TADF) emitters,[174–178] and π-conjugated bioorganic (BIO) molecules.[72,115,179–212] Molecules in the PAH, OPV, and BIO sets possess locally excited T_1 and S_1 states with different extents of delocalized π-bonds, while TADF emitters have charge transfer T_1 and S_1 states. The structures of all molecules are listed in Figs. S1–S9 in the Supporting Information, and representative species are provided in Fig. 1.

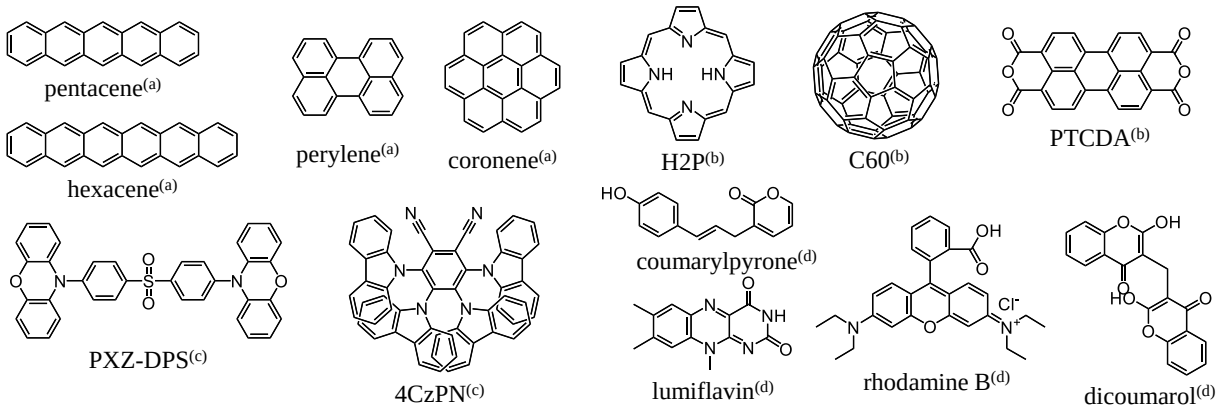

Figure 1: Representative molecules from the test sets of (a) PAH, (b) OPV, (c) TADF, and (d) BIO.

2.5 Computational Details

With nuclear relaxation in consideration, we evaluated E_{T}, E_{S}, and ΔE_{ST} under three geometric variants, "absorption" (abs), "emission" (em) and "adiabatic" (adi) (Fig. 2), and compared each of them to its experimental counterpart. $I_{\perp}$, $A_{\perp}$, $-\varepsilon^{(N)}_{\mathrm{HOMO}}$, and $-\varepsilon^{(N+1)}_{\mathrm{HOMO}}$ were evaluated at the S_0 geometry. In all cases, the molecular configurations associated with S_0 and T_1 were optimized using RDFT with $M_S = 0$ and UDFT with $M_S = \pm 1$ respectively,[213] while those of the first singlet excited states (S_1) were optimized using ROKS.[8] All geometry optimizations utilized the B3LYP functional.[60,213,214] System-dependent ω and C_{HF} were *non-empirically* tuned at the optimized S_0 geometries by minimizing Eqs. (4), (10), or (13). For single-parameter versions of TT-ωPBEh, we optimized C_{HF} at $\omega = 0.200 a_0^{-1}$ (TT-ωPBEhω, $a_0 \equiv$ bohr), or optimized ω at $C_{\mathrm{HF}} = 0.20$ (TT-ωPBEhC), by performing a gold-section search of the one-dimensional minimum.[215,216] For TT-ωPBEh, OT-ωPBEh, and mix-ωPBEh with tunable ω and C_{HF}, two-dimensional minimizations were carried out using the simplex algorithm.[216]

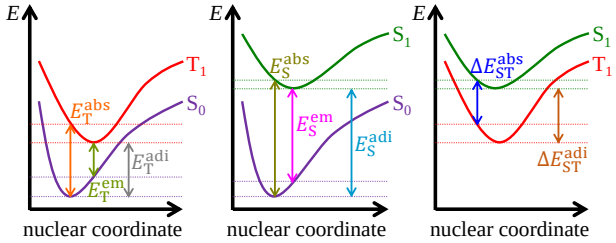

Figure 2: Geometric variants of E_{T}, E_{S}, and ΔE_{ST} applied in the present study. "Abs", "em" and "adi" represent the absorption, emission, and adiabatic energy gaps.

Based on the optimized values of ω and C_{HF}, E_{T}, E_{S}, ΔE_{ST}, and $I_{\perp}$ were evaluated using single-point ΔSCF, TDDFT, and ROKS. For molecules that suffer from failed diagonalization of the linear-response matrix, the Tamm–Dancoff approximation (TDA)[217] was included in the TDDFT calculations. $\varepsilon_{\mathrm{HOMO}}^{(N)}$ and $\varepsilon_{\mathrm{HOMO}}^{(N+1)}$ were extracted as eigenvalues of KS orbitals produced in the ground-state calculations of neutral and anionic species. All such single-point energies were compared with the experimental measurements performed at the appropriate geometric variants shown in Fig. 2, and the accuracy was described using the absolute error (AE):

$$\mathrm{AE}(X) = \left| E_X^{\mathrm{calc}} - E_X^{\mathrm{expt}} \right|. \tag{14}$$

If more than one geometric variants for any species are experimentally available, we averaged these AEs . The accuracy of any XC functional was calibrated using the mean absolute error (MAE) that was averaged over all molecules within each test set.

Besides OT-ωPBEh, ten existing functionals were also compared with TT-ωPBEh and mix-ωPBEh, including HF,[57] B3LYP,[218] CAM-B3LYP,[26] PBE,[63] PBE0,[219] LRC-ωPBE ($\omega = 0.300a_0^{-1}$ and $C_{\mathrm{HF}} = 0.00$),[31] LRC-ωPBEh ($\omega = 0.200a_0^{-1}$ and $C_{\mathrm{HF}} = 0.20$),[33] TPSS,[22] M06-2X,[25] and M06-L.[24] All calculations reported in the present study used the cc-pVDZ basis set[220] and the Q-Chem 4.4 package.[221]

3 Results and Discussions

3.1 Optimized Parameters

3.1.1 Necessity of Double Parameters

In the current subsection, we will show the necessity to set both ω and C_{HF} as tunable in TT-ωPBEh by presenting the insufficiency of TT-ωPBEhω and TT-ωPBEhC based on two oligomer series from our test sets: oligoacenes ($n = 1 - 6$, PAH) and α-oligothiophenes ($n = 1 - 7$, OPV).

The reciprocal of ω (ω^{-1}) provides the interelectron distance where the short-range PBE–HF

hybrid exchange transitions to the long-range pure HF exchange. A small ω represents a small overall HF fraction, and *vice versa*. Fig. 3(a) illustrates optimal ω^{-1} for TT-ωPBEhω for both oligomer series. Although the trend of the overall HF fraction is not obvious for either series except for an increase in larger α-oligothiophenes ($n \geq 5$), a large ω^{-1} ($\omega^{-1} > 100a_0$) in optimized TT-ωPBEhω indicate a negligible HF contribution, or more possibly, the non-existence of a minimum on the one-dimensional surface of $J_{\mathrm{TT}}^2(\omega)$ at a typical value of $C_{\mathrm{HF}} = 0.20$. Similarly, TT-ωPBEhC presents a constant of $C_{\mathrm{HF}} = 0.00$ for both oligomer series (Fig. 3(b)), also showing the difficulty in finding the optimal C_{HF} at a typical value of $\omega = 0.200a_0^{-1}$.

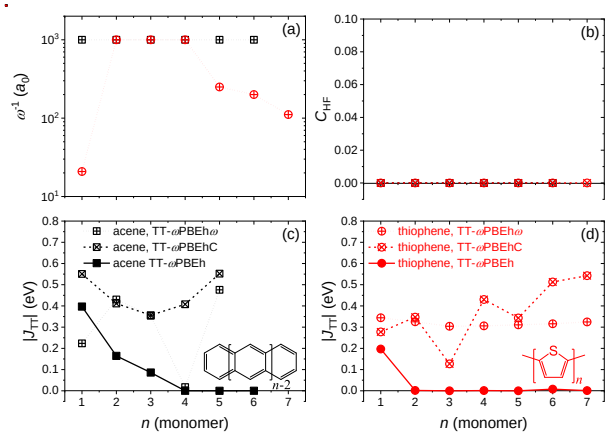

Figure 3: (a) Optimized ω^{-1} (a_0^{-1}) in TT-ωPBEhω ($C_{\mathrm{HF}} = 0.20$, hollow with plus) for oligoacenes (black square) and α-oligothiophenes (red circle). (b) Optimized C_{HF} in TT-ωPBEhC ($\omega = 0.200a_0^{-1}$, hollow with cross) for oligoacenes and α-oligothiophenes. (c) Minimized $|J_{\mathrm{TT}}|$ (eV) for oligoacenes using TT-ωPBEhω, TT-ωPBEhC, and TT-ωPBEh (solid). (d) Minimized $|J_{\mathrm{TT}}|$ for α-oligothiophenes using TT-ωPBEhω, TT-ωPBEhC, and TT-ωPBEh.

To evaluate how well the exact triplet tuning constraint (Eq. (3)) is satisfied by TT-ωPBEhω, TT-ωPBEhC, and TT-ωPBEh under optimized ω or C_{HF}, we also compare the value of $|J_{\mathrm{TT}}|$, the square root of the minimized J_{TT}^2 (Eq. (4)), in Fig. 3(c) and (d). TT-ωPBEhω and TT-ωPBEhC both exhibit huge $|J_{\mathrm{TT}}|$'s for most molecules (as large as $\simeq$0.6 eV), while TT-ωPBEh presents very small $|J_{\mathrm{TT}}|$'s (< 0.1 eV) except for the smallest benzene, naphthalene, and thiophene. This observation further validates that a reasonable minimum of J_{TT}^2 *does not necessarily exist* unless at least two parameters are used in the triplet tuning procedure.

3.1.2 Independent Parameters

As both ω and C_{HF} are related to the overall fractions of PBE and HF in our long-range-corrected (LRC) hybrid formula, it is necessary to eliminate any possible correlation between ω and C_{HF} for TT-ωPBEh. In Fig. 4 we summarize optimized ω and C_{HF} for all molecules in question. For the majority of species, $\omega < 0.5a_0^{-1}$, indicating that the long-range HF exchange usually takes effect when $r_{12} > 2a_0$. In addition, C_{HF} can range from 0 to 1, but most molecules need $C_{\mathrm{HF}} < 0.4$ to reach the desired accuracy.

To satisfy Koopmans' theorem, molecules with similar chromophoric sizes are expected to possess similar overall HF exchange fractions. Therefore in OT-ωPBEh a smaller value of ω is usually compensated by a larger value of C_{HF}, and this expected negative correlation is presented in Fig. 4(b). For TT-ωPBEh, on the other hand, ω and C_{HF} are statistically independence from each other (Fig. 4(a)) and can thus be *non-empirically* and *mutually* tuned, and molecules with similar-sized chromophores might end up with very different sets of optimized parameters.

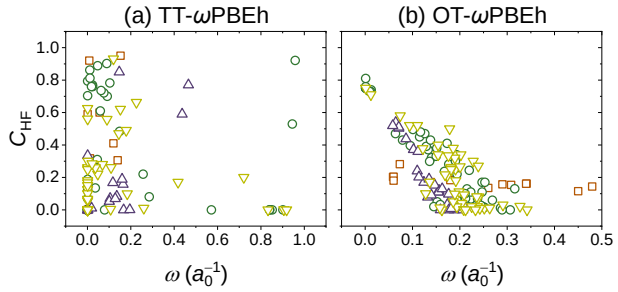

Figure 4: Correlation between optimized ω (a_0^{-1}) and C_{HF} for (a) TT-ωPBEh and (b) OT-ωPBEh.

3.2 Triplet Excitation Energy

As was mentioned in Secs. 1 and 2, our proposed TT-ωPBEh functional arrives at a *non-empirical* matching of E_{T} between ΔSCF and TDDFT (Eq. (3)). Accordingly the accuracy of E_{T} becomes a natural calibration of TT-ωPBEh. Given the well-minimized J^2_{TT}, we expected TT-ωPBEh to reach the best approximation of the exact XC functional and thus to provide the most accurate prediction of E_{T} among all XC functionals in comparison, especially for badly-behaved molecules with large-

scale π-conjugations or significant charge transfer excitations. Because TT-ωPBEh allows us to evaluate ω and C_{HF} *independently* from any experimental measurements, it presents a minimal fitting artifact and can be safely compared to experiments.

As was described in Sec. 2, the error of a functional is characterized using its MAEs. We report the MAEs of E_{T}'s using three single-point DFT variants: ΔSCF, TDDFT, and TDDFT/TDA (Tables S1, S5, S9, and S11). We also summarize TDDFT-evaluated MAEs in the left part of Table 1. In these tables and those that follow, the **bold**, underlined, and *italic* numbers represent the smallest, second smallest, and largest MAEs within each column, respectively.

In an ideal situation, all DFT variants provide identical values for E_{T}. However, this is difficult to accomplish as the minimized J_{TT}^2 can hardly reach a rigorous zero. To quantify the error arising from a non-zero J_{TT}^2, as well as to characterize the lower and upper bounds of MAEs, for every single molecule we evaluated E_{T} using all three variants and picked the best and worst results (the smallest and largest AEs). The averages of these *best* and *worst* AEs were defined as the *best* and *worst* MAEs, respectively, and are included along with their differences for all E_{T}'s in Tables S1, S5, S9, and S11. *Worst* MAEs are summarized in the right part of Table 1.

In addition, it is worthwhile to make a systematic comparison between our proposed TT-ωPBEh and existing functionals, especially the very popular hybrid B3LYP,[60,213,214] PBE,[63] and PBE0[219] in the last two decades. Therefore we defined

$$\Delta\mathrm{AE}_A = \mathrm{AE}_A - \mathrm{AE}_{\mathrm{TT}-\omega\mathrm{PBEh}} \tag{15}$$

and present molecules with significant $\Delta\mathrm{AE}_{\mathrm{B3LYP}}$'s and $\Delta\mathrm{AE}_{\mathrm{PBE0}}$'s in Figs. 5 and S11 evaluated using the *best* AE from TT-ωPBEh.

3.2.1 Locally Excited Triplet State

In the present subsection, we will show the excellent performance of TT-ωPBEh for the test sets of PAH, OPV, and BIO. Each of these molecules possesses a moderate- or large-scale π-conjugation

Table 1: MAEs (eV) of E_T's are compared across various functionals for all test sets.[a]

energy	TDDFT				*worst*			
XC functional	PAH	OPV	TADF	BIO	PAH	OPV	TADF	BIO
TT-ωPBEh	**0.158**	**0.219**	0.258	0.239	**0.226**	**0.362**	**0.298**	**0.310**
OT-ωPBEh	0.315	0.432	**0.212**	0.365	0.397	0.534	0.374	0.527
mix-ωPBEh	0.306	*0.489*	0.341	0.404	0.428	0.592	0.474	0.547
HF	0.235	0.290	0.288	0.272	*0.771*	*1.078*	*1.077*	*0.869*
B3LYP	0.255	0.322	0.272	0.313	0.331	0.367	0.324	0.356
CAM-B3LYP	0.244	0.374	0.298	0.350	0.330	0.480	0.545	0.445
PBE0	0.331	0.310	0.236	0.340	0.392	0.884	0.316	0.406
LRC-ωPBE	*0.367*	0.390	0.299	*0.428*	0.455	0.516	0.700	0.514
M06-2X	0.206	0.274	*0.352*	**0.192**	0.405	0.444	0.557	0.322

[a] **Bold**, underlined, and *italic* numbers represent the smallest, second smallest, and largest MAEs within each column.

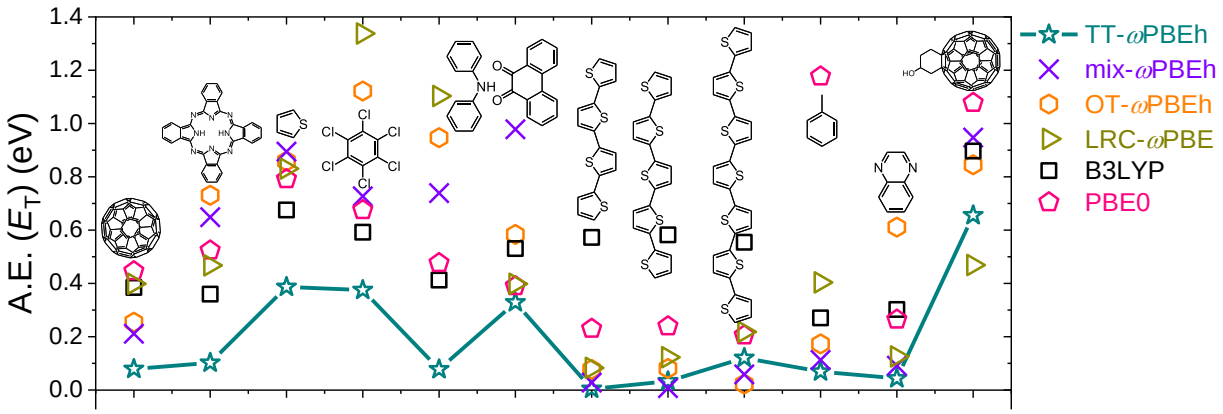

Figure 5: AEs of E_T's (eV) are illustrated for selected OPV materials. The results are compared among TT-ωPBEh (dark cyan star), mix-ωPBEh (violet cross), OT-ωPBEh (orange hexagon), LRC-ωPBE (dark yellow right triangle), B3LYP (black square), and PBE0 (pink pentagon).

over its chromophore and a *locally excited* T_1 state. Based on Tables 1 and S1, S5, S9, and S11, as well as Figs. 5 and S11, TT-ωPBEh achieves the most accurate predictions of E_T's among all XC functionals in question.

For PAH and OPV sets, using TDDFT TT-ωPBEh provides the smallest MAE, outperforming any other functionals including B3LYP and PBE0. Especially, OT-ωPBEh and mix-ωPBEh demonstrate doubled MAEs from TT-ωPBEh, indicating their expected inferior performances (Sec. 3.1.2) to TT-ωPBEh (Figs. 5 and S11). A similar trend was observed for BIO molecules as well (outperformed by M06-2X only). In addition, although TT-ωPBEh does not necessarily provide the

smallest *best* MAEs, its *worst* counterparts are always superior to every other functional across all molecule sets. Also, TT-ωPBEh exhibits on average the smallest difference between *worst* and *best* MAEs, validating the best satisfaction of the triplet tuning constraint (Eq. (3)).

Combining these two results, we can draw two major conclusions: (1) TT-ωPBEh reproduces the most accurate electron-hole interactions and accomplishes the best approximation to the exact functional and the best stability across DFT variants when applying to a locally excited T_1 state. (2) The consideration of Koopmans' theorem deteriorates this advantage and make OT-ωPBEh and mix-ωPBEh worse than non-tuned functionals like B3LYP and PBE0. Based on these conclusions, we can assert that TT-ωPBEh is advantageous over other functionals for locally excited T_1 states.

In a systematic comparison, we found a large fraction of molecules where TT-ωPBEh exhibits significant advantages over B3LYP and PBE0. For instance, more than one third of OPV materials in question exhibit $\Delta \mathrm{AE}_{\mathrm{B3LYP}} > 0.20$ eV and are shown in Fig. 5. Configurationally, most molecules illustrated here possess very extensive π-conjugations in one (like α-oligothiophene) or two dimensions (like fullerene), for which the locality of LDA and GGA components in B3LYP and PBE0 are known to introduce a serious SIE and thus an inaccurate E_{T}.[9–17] However, the LRC and triplet tuned formula of TT-ωPBEh minimizes the SIE in both short and long ranges[30–38] and reaches the best accuracy of low-lying T_1 states. Also, the *non-empiricism* of TT-ωPBEh shows no bias towards any species and makes it robust for newly-synthesized molecules that are not yet included in any fitting database.

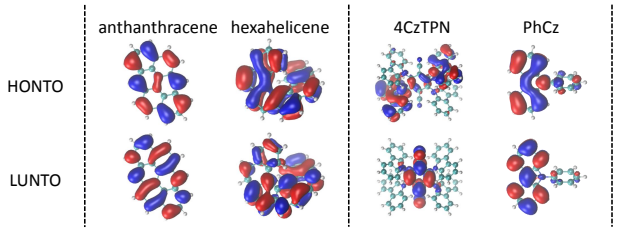

Figure 6: HONTO and LUNTO of the T_1 state for anthanthracene and hexahelicene from PAH (left), and 4CzTPN and PhCz from TADF (right).

Finally, to depict the locality of T_1 states discussed in the present subsection, we illustrate the perfect spatial overlaps between the highest occupied NTO (HONTO) and the lowest unoccupied

NTO (LUNTO) in the left panel of Fig. 6 for two selected PAH molecules, anthanthracene and hexahelicene. For a similar locally excited T_1 state the accuracy of TT-ωPBEh can be guaranteed.

3.2.2 Charge Transfer Triplet State

In the present subsection, we will show that TT-ωPBEh exhibits a strong predictive power for a *charge transfer* T_1 state which is essentially a pseudo-one-particle property, such as that of a TADF emitter.

OT-ωPBEh was constructed to largely reduce the SIE associated with a charge transfer excited state,[9–17,34,37,38] and it proves to exhibit the smallest MAE as expected (Tables 1 and S9). Interestingly, arriving at an analogous long-range HF exchange,[222–224] TT-ωPBEh shows a comparable predictive power to OT-ωPBEh and PBE0, and a smaller AE than B3LYP for three quarters of TADF emitters. Meanwhile, the *worst* MAE of TT-ωPBEh is still the smallest of all, while OT-ωPBEh is even outperformed by non-tuned B3LYP and PBE0. Although the ordinary performance of mix-ωPBEh indicates a difficulty in coordinating the electron-hole interaction and the asymptotic density using the same set of parameters, the *unexpected* excellent performance of TT-ωPBEh indicates the gain of complying with Eq. (3) at only a tiny cost of the long-range behavior. In conclusion, TT-ωPBEh is still the best functional on balance even for a charge transfer system for which OT-ωPBEh was originally designed.

To extend our discussion, we also explored the sensitivity of TT-ωPBEh on T_1 to the charge separation extent in the space.[9–16,225] Due to the SIE and the inaccurate adiabatic local density approximation (ALDA) in TDDFT, poor performance is expected for a severe charge transfer T_1 state using TT-ωPBEh. To visualize our argument, we illustrate HONTO and LUNTO for the T_1 states of two TADF emitters, 4CzTPN and PhCz, in the right panel of Fig. 6. 4CzTPN exhibits a strong charge transfer character and its TDDFT-evaluated AE using TT-ωPBEh (0.608 eV) is three times as much as that using OT-ωPBEh (0.205 eV), while for a minimally charge-separated PhCz the performance of TT-ωPBEh is significantly better (0.038 eV versus 0.364 eV). To treat molecules like 4CzTPN, one should consider a methodological modification like to incorporate the

frequency dependence in E_{XC}[226–228] or to implement the multi-configurational therapy.[17,229,230]

3.3 Optical Band Gap

In spite of not being the direct tuning object, E_{S} is a more interesting observable than E_{T} and an independent benchmark of TT-ωPBEh as it can be directly measured via absorption or fluorescence spectroscopy with abundant data available in the literature. For a normal closed-shell molecule, E_{S} is the energy difference between S_0 and S_1 (which possesses an identical orbital configuration to T_1). Therefore TT-ωPBEh is expected to provide an accurate prediction for E_{S}.

Table 2: MAEs (eV) of E_{S}'s are compared across various functionals for all test sets.[a]

energy	TDDFT				*worst*			
XC functional	PAH	OPV	TADF	BIO	PAH	OPV	TADF	BIO
TT-ωPBEh	0.381	**0.316**	**0.266**	<u>0.370</u>	0.581	0.661	**0.357**	<u>0.571</u>
OT-ωPBEh	0.343	0.510	<u>0.338</u>	0.506	0.563	0.724	0.465	0.720
mix-ωPBEh	0.331	0.414	0.352	0.584	0.518	0.673	0.504	0.889
HF	*0.774*	*0.793*	*1.792*	*1.292*	0.774	*0.793*	*1.792*	*1.358*
B3LYP	**0.276**	<u>0.396</u>	0.390	**0.309**	0.525	0.590	<u>0.416</u>	**0.432**
PBE	0.416	0.507	1.017	0.456	0.741	0.792	1.023	0.614
LRC-ωPBE	0.494	0.525	0.768	0.545	*0.854*	0.716	0.907	0.773
LRC-ωPBEh	0.348	0.430	0.627	0.499	**0.463**	**0.540**	0.651	0.635
M06-2X	<u>0.312</u>	0.437	0.477	0.466	<u>0.484</u>	<u>0.569</u>	0.499	0.605

[a] **Bold**, <u>underlined</u>, and *italic* numbers represent the smallest, second smallest, and largest MAEs within each column.

We summarize all MAEs for E_{S}'s in Tables S2, S6, S10, and S12, including the *best* and *worst* MAEs as defined in Sec. 3.2, except that ROKS is in place of ΔSCF. In Table 2 we list the TDDFT-evaluated and *worst* MAEs. In Figs. 7 and S12, we visualize the comparison of *best* AEs for selected molecules with large $\Delta\mathrm{AE}_{\mathrm{B3LYP}}$'s ($> 0.20$ eV except for DTC-DPS) and $\Delta\mathrm{AE}_{\mathrm{PBE}}$'s ($> 0.40$ eV).

3.3.1 Transferability from Triplet to Singlet

As we can expect in advance, TT-ωPBEh always provides a larger MAE for E_{S} than E_{T}. Due to the orbital similarity between S_1 and T_1, TT-ωPBEh exhibits the strongest predictive power of E_{S}

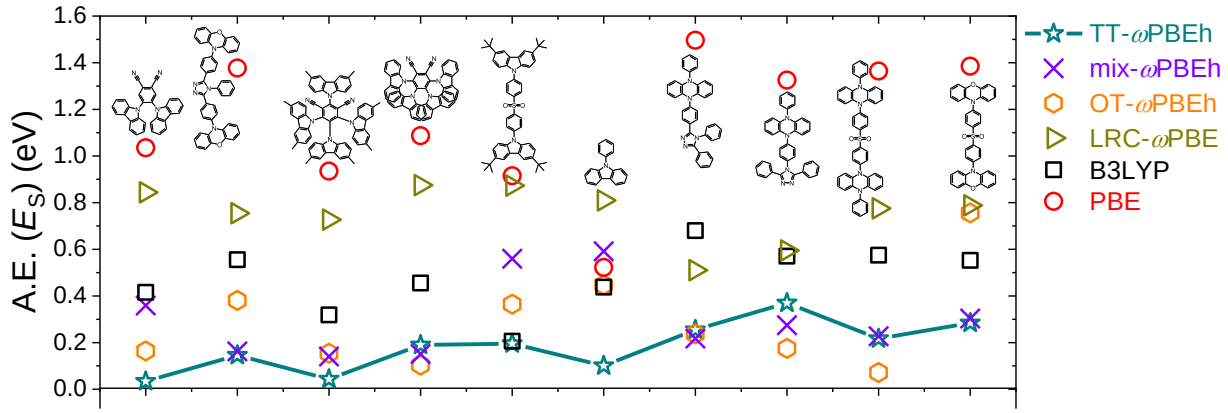

Figure 7: AEs of E_{S}'s (eV) are illustrated for selected TADF emitters. The results are compared among TT-ωPBEh (dark cyan star), mix-ωPBEh (violet cross), OT-ωPBEh (orange hexagon), LRC-ωPBE (dark yellow right triangle), B3LYP (black square), and PBE (red up triangle).

for the OPV and TADF sets, and the second strongest for BIO molecules (outperformed by B3LYP only). Especially, for TADF emitters TT-ωPBEh displays its superiority across all DFT variants (including *best* and *worst* MAEs). This discovery is *shocking* but not completely unexpected – it can be explained by the small ΔE_{ST} between charge transfer S_1 and T_1 states with negligible spatial overlaps between HONTO and LUNTO. These results confirm the suggested transferability of TT-ωPBEh from a difficult observable, E_{T}, to an easy one, E_{S}, especially for a compound with a charge transfer S_1 state. Such a transferability sets the stage for the usage of TT-ωPBEh in large-scale screening and design of spectroscopically and photochemically active materials.

Similar to the assessment in Sec. 3.2, an explicit comparison was also made for E_{S} between TT-ωPBEh and popular functionals. Ten out of the twelve TADF emitters show positive $\Delta\mathrm{AE}_{\mathrm{B3LYP}}$'s and $\Delta\mathrm{AE}_{\mathrm{PBE}}$'s and are illustrated in Fig. 7. The poor performance of B3LYP and PBE on these charge transfer molecules can also be interpreted by their significant SIEs.

3.3.2 Singlet–Triplet Instability Problems

TT-ωPBEh consistently overestimates E_{S} for PAH molecules using TDDFT. Its MAE is larger than a handful of functionals including B3LYP, PBE, and LRC-ωPBEh (Table 2). The singlet–triplet instability problem is associated with the linear-response formulation that significantly underestimates E_{T} and overestimates E_{S} and is the probably the most substantial contribution to this

error,[231] as parameters optimized by matching such underestimated $E_{\mathrm{T}}^{\mathrm{TDDFT}}$ with $E_{\mathrm{T}}^{\Delta\mathrm{SCF}}$ can definitely lead to an overestimated E_{S}. The inclusion of TDA[217] in TDDFT can numerically eliminate the instability, but it even increases the MAE if TDA is not implemented in the triplet tuning procedure. This issue indicates a modification strategy to replace $E_{\mathrm{T}_1}^{\mathrm{TDDFT}}$ in Eq. (2) with $E_{\mathrm{T}_1}^{\mathrm{TDDFT/TDA}}$ for molecules affected by the instability problem so that the tuning will arrive at a better set of parameters.

3.4 Singlet–Triplet Gap in a Charge Transfer System

In a TADF system, ΔE_{ST} serves as a direct predictor for the (reversed) intersystem crossing rate ($k_{(\mathrm{R})\mathrm{ISC}}$) and the quantum yield (ϕ) of the emitter.[232] The accuracy of ΔE_{ST} proved very sensitive to the level of theory[174,233–237] and is then an additional benchmark of TT-ωPBEh. In the present subsection, we will show that TT-ωPBEh maintains an exceptional prediction for ΔE_{ST}.

Table 3: MAEs (eV) of ΔE_{ST}'s are compared across various functionals for the TADF test set.[a,b]

XC functional	ΔSCF/ROKS	TDDFT	TDDFT/TDA	*best*	*worst*
TT-ωPBEh (gas)	<u>0.298</u>	0.298	0.297	0.227	<u>0.362</u>
TT-ωPBEh (PCM)	0.309	**0.268**	0.278	**0.118**	0.447
OT-ωPBEh (gas)	<u>0.298</u>	0.310	**0.208**	<u>0.156</u>	0.381
OT-ωPBEh (PCM)	*0.456*	0.314	0.292	0.220	0.551
mix-ωPBEh (gas)	0.355	0.463	0.345	0.233	0.526
mix-ωPBEh (PCM)	0.392	0.361	<u>0.237</u>	<u>0.156</u>	0.525
HF	-	*1.487*	*1.487*	*1.487*	*1.487*
B3LYP	**0.226**	<u>0.279</u>	0.305	0.186	**0.358**
LRC-ωPBE	0.360	0.672	0.349	0.242	0.727
LRC-ωPBEh	-	0.567	0.285	0.271	0.581
TPSS	-	0.375	0.381	0.372	0.384
M06-L	-	0.365	0.376	0.360	0.382

[a] **Bold**, <u>underlined</u>, and *italic* numbers represent the smallest, second smallest, and largest MAEs within each column.
[b] "Gas" and "PCM" represent single-point calculations performed in the gas phase and using the PCM solvent model.

In Table 3, we illustrate MAEs of ΔE_{ST}'s for TADF emitters evaluated using different DFT variants as well as *best* and *worst*. As was discussed in Sec. 3.2.2, although TT-ωPBEh does

not implement Koopmans' theorem,[40] its long-range HF exchange allows its accuracy to approach that of OT-ωPBEh.[222] Analogously for ΔE_{ST}, the values of $|\Delta \mathrm{AE}_{\mathrm{OT}-\omega\mathrm{PBEh}}| < 0.09$ eV across all single-point DFT variants and TT-ωPBEh exhibits the second lowest *worst* MAE. On the other hand, the non-LRC B3LYP functional also shows outstanding performance due to the error cancellation between E_{S} and E_{T}, which is however viewed as an unreliable coincidence. Taking these results into account, TT-ωPBEh reaches the strongest and most stable predictive power for ΔE_{ST}.

3.4.1 Solvation Effect

Due to large permanent dipole moments, S_1 and T_1 of a TADF emitter can both be stabilized in a polarized solvent, leading to an unpredictable shift of ΔE_{ST}.[233–236] Also, the experimental measurements cited in the present study were carried out in the condensed phase (solutions or aggregates).[175–177] In recent studies,[174,237] the solvation effect was modeled using the implicit polarizable continuum model (PCM), in which the dielectric constant of the environment, ε, rescales all electric effects. However, the involvement of even the simplest PCM significantly increases the computational cost, and therefore it was not used in our triplet tuning process.

This issue motivated us to find an inexpensive way of including the solvation effect. Based on gas-phase-optimized parameters, we re-evaluated ΔE_{ST} in toluene ($\varepsilon = 2.38$) using PCM (labeled accordingly in Table 3). This treatment improves, or at least *does not compromise*, the accuracy of TT-ωPBEh and mix-ωPBEh as the polarized environment increases the charge transfer extent that was underestimated by the gas-phase triplet tuning process. On the contrary, OT-ωPBEh already overestimated the charge transfer extent in the gas phase, so the implementation of the solvation effect plays an adverse role. Our findings suggest a future direction that incorporates the solvation effect in the construction of TT-ωPBEh such as replacing r_{12} with εr_{12} in the Hamiltonian.[47,238–240]

3.5 Spin Contamination

Although we have shown the excellent performance of TT-ωPBEh in E_{T}, E_{S}, and ΔE_{ST}, the spin contamination problem of UDFT still implies an additional source of error. UDFT constrains

$M_S = \pm 1$ for a triplet state but loses control of $\langle S^2 \rangle$. In the present study, we defined a UDFT-evaluated T_1 to be spin pure when $1.95 < \langle S^2 \rangle < 2.05$. This criterion is satisfied in our test sets, except for a few TADF emitters that are mixed with higher spin configurations. Such spin contamination usually occurs at a large HF fraction (large C_{HF} and large ω) or in a strongly-correlated or multi-radical system.[241–243] For instance, T_1 of 4CzTPN displays a vast spatial separation between HONTO and LUNTO under TT-ωPBEh ($\omega = 0.147 a_0^{-1}$ and $C_{\mathrm{HF}} = 0.85$), and thus can be treated as a *diradical* structure (Fig. 6). UDFT produces $\langle S^2 \rangle = 2.3358$, equivalent to a superposition of 92% triplet and 8% quintet ($\langle S^2 \rangle = 6$). Its TDDFT-evaluated AEs are 0.618 eV, 1.633 eV, and 1.025 eV for E_{T}, E_{S}, and ΔE_{ST}, respectively, all being huge.

In an attempt to resolve this problem, we re-evaluated E_{T_1} for spin-contaminated molecules using restricted open-shell DFT (RODFT) but still UDFT-tuned parameters. However, this short-term fix raised the computational cost by one order of magnitude and increased the AEs by more than 1 eV as it introduces extra difficulty to the variational calculation while imposing the additional spin symmetry. The long-term therapy in the frame of single-reference DFT is to replace $E_{\mathrm{T}_1}^{\mathrm{UDFT}}$ in Eq. (1) with $E_{\mathrm{T}_1}^{\mathrm{RODFT}}$ to ensure the spin purity of T_1, but the above-mentioned convergence difficulty makes it beyond the scope of the present study due to technical limitation.

3.6 One-Electron Property

The observable one-particle property, $I_\perp$, affords an additional benchmark for TT-ωPBEh. In the present subsection, we will compare $-\varepsilon_{\mathrm{HOMO}}^{(N)}$ to experimental $I_\perp$'s (I_{expt}) for various functionals and will show the superiority of TT-ωPBEh over non-LRC functionals like B3LYP and M06-L. Herein the difference between $-\varepsilon_{\mathrm{HOMO}}^{(N)}$ and I_{expt} is defined as the AE. All MAEs are listed in Tables S3, S7, and S13, and those from $-\varepsilon_{\mathrm{HOMO}}^{(N)}$'s are reported for the PAH, OPV, and BIO sets in Table 4. The $-\varepsilon_{\mathrm{HOMO}}^{(N)}$ versus I_{expt} relation for selected OPV materials is displayed in Fig. 8.

As we foresaw earlier, because of the incorrect long-range nature, $-\varepsilon_{\mathrm{HOMO}}^{(N)}$ is consistently underestimated by all non-LRC functionals (B3LYP, PBE, TPSS, and M06-L), which also loses the predictive power for $I_\perp$. Like all existing optimally tuned functionals,[37,41,42,244–246] OT-ωPBEh

Table 4: MAEs (eV) of $-\varepsilon_{\mathrm{HOMO}}^{(N)}$'s are compared across various functionals for the test sets of PAH, OPV, and BIO.[a]

XC functional	PAH	OPV	BIO
TT-ωPBEh	1.182	1.737	2.037
OT-ωPBEh	<u>0.174</u>	<u>0.213</u>	0.352
mix-ωPBEh	0.191	**0.173**	<u>0.327</u>
HF	0.394	0.298	0.429
B3LYP	1.901	2.055	2.472
PBE	2.446	*2.868*	*3.355*
LRC-ωPBE	**0.170**	0.231	**0.177**
TPSS	*2.500*	2.857	3.323
M06-L	2.354	2.661	2.980

[a] **Bold**, <u>underlined</u>, and *italic* numbers represent the smallest, second smallest, and largest MAEs within each column.

was constructed based on Koopmans' theorem[40] and exhibits expected excellent performance. Meanwhile, although the accuracy of TT-ωPBEh is surpassed by HF and other LRC functionals (OT-ωPBEh, mix-ωPBEh, and LRC-ωPBE), it is significantly better-behaving than all non-LRC functionals due to its correct asymptotic behavior, and it presents an overestimated $-\varepsilon_{\mathrm{HOMO}}^{(N)}$ rather than an underestimation when the overall HF fraction is higher than usual.

More interestingly, mix-ωPBEh has an *unexpectedly* comparable performance to OT-ωPBEh and its MAEs are even smaller than OT-ωPBEh for OPV and BIO sets, indicating that using mix-ωPBEh we can obtain equally good $I_\perp$ as those using OT-ωPBEh without sacrificing the accuracy for E_{T} and E_{S}. This result suggests the combination of the ideas of Koopmans-based optimal tuning and our proposed triplet tuning leads to a correct direction to the mutual treatment of electron-hole interactions and one-particle properties – within a two-dimensional parameter space, these two targets are no longer incompatible with each other.

The discussion we have conducted so far in Sec. 3 allows us to safely assert the value of the fully and partially triplet tuned XC functionals like TT-ωPBEh and mix-ωPBEh in the accurate prediction of spectroscopically and photochemically important excited states.

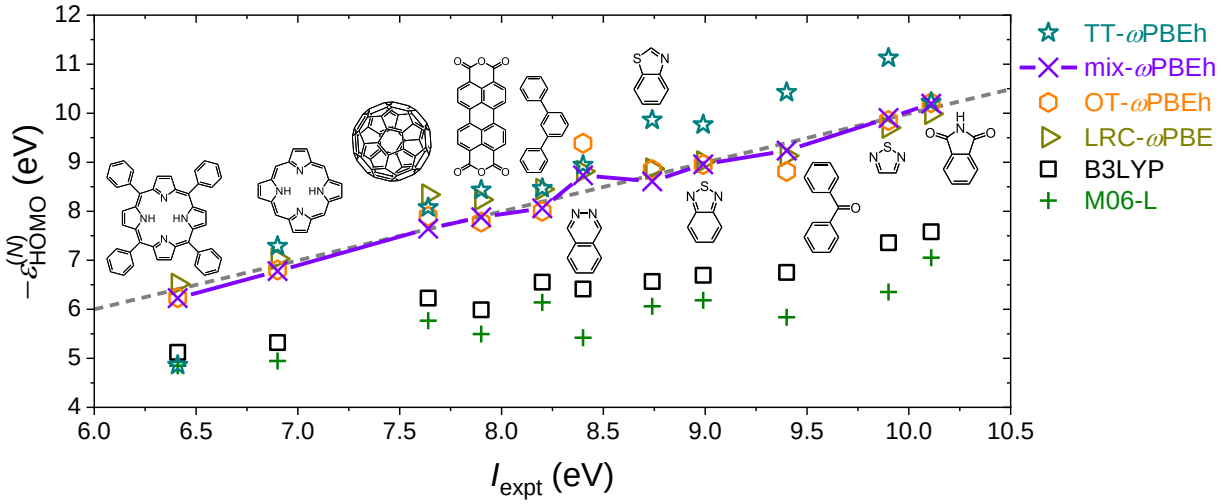

Figure 8: $-\varepsilon^{(N)}_{\mathrm{HOMO}}$'s (eV) are compared against I_{expt}'s (eV) for selected OPV materials. The results are presented for TT-ωPBEh (dark cyan star), mix-ωPBEh (violet cross), OT-ωPBEh (orange hexagon), LRC-ωPBE (dark yellow right triangle), B3LYP (black square), and M06-L (green plus). The Koopmans' theorem[40] is illustrated as the diagonal grey dashed line.

4 Conclusion and Future Directions

In the present study, we proposed triplet tuning, a novel prescription that allows us to construct an approximate XC functional based on the energy of T_1 (E_{T}), in a *non-empirical* manner. The first triplet-tuned functional, TT-ωPBEh, was constructed by an internal matching of E_{T} from two DFT variants, ΔSCF and TDDFT. To evaluate the behavior of TT-ωPBEh, we compared its errors for E_{T}, E_{S}, ΔE_{ST}, and $-\varepsilon^{(N)}_{\mathrm{HOMO}}$ against existing functionals, including the most popular B3LYP, PBE, PBE0, and one using the conventional optimal tuning scheme, OT-ωPBEh. Without fitting to *any* experimental data, TT-ωPBEh provides an accurate prediction of electron-hole interactions in a π-conjugated organic molecule and is in general significantly more powerful than other functionals in photochemically interesting energetics like E_{T}, E_{S}, and ΔE_{ST} . On the other hand, TT-ωPBEh also improves the accuracy of one-electron properties like $-\varepsilon^{(N)}_{\mathrm{HOMO}}$ relative to any (semi-)local, non-LRC functional. In the end, given the difficulty of balancing local electron-hole interactions and non-local one-electron properties, the mix-ωPBEh functional that grants both aspects has achieved *unexpected* accuracy for $-\varepsilon^{(N)}_{\mathrm{HOMO}}$.

Similar to conventional optimally tuned functionals,[247–256] we expected a broad application of

our triplet tuning approach for π-conjugated organic molecules that were considered theoretically challenging before. Beyond the accurate predictions of spectroscopy and dynamics, the method can set the stage for the computationally aided design and screening of photoactive materials. In parallel projects being conducted in our group, the present version of TT-ωPBEh has been applied to molecules and clusters that are involved in singlet fission and photoluminescence.

As discussed in Sec. 3, there is room for non-trivial development of the present triplet tuning scheme so as to strengthen its predictive power for difficult excited states. For example, the present LRC hybrid formula of HF and PBE[63] turns out inaccurate for some PAH molecules and TADF emitters, and ω and C_{HF} do not necessarily span a large enough two-dimensional space that contains the exact exchange functional. To resolve these issues without touching the current framework of single-reference DFT, we can reformulate the present triplet-tuned functionals by using alternative formulas or adjustable parameters. For example, we can include the environmental factors such as ε of the solvent and the intermolecular interactions,[237,257] or we can develop functionals that depend on the frequency[226,227] and the local electronic density.[258] Finally, to accelerate the tuning process we can implement alternative minimization algorithms and apply the data-driven idea like machine learning.[259,260]

5 Associated Content

In the Supporting Information, we provide the structures for all organic molecules that are included in the four test sets under investigation, the discussion about parameter convergence, the tables and figures that summarize AEs and MAEs, and the statistical analysis for all functionals. This information is available free of charge via the Internet at http://pubs.acs.org.

6 Acknowledgment

Z. L. and T. V. thank the National Science Foundation for the support of the present study (Grant CHE-1464804). We also thank Prof. Leeor Kronik, Prof. Roi Baer, Dr. Tianyu Zhu, Dr. Xing

Zhang, and Mr. Diptarka Hait for inspirational and insightful discussions.

References

(1) Hohenberg, P.; Kohn, W. Inhomogeneous Electron Gas. *Phys. Rev.* **1964**, *136*, B864–B871.

(2) Kohn, W.; Sham, L. J. Self-Consistent Equations Including Exchange and Correlation Effects. *Phys. Rev.* **1965**, *140*, A1133–A1138.

(3) Parr, R. G.; Yang, W. *Density-functional theory of atoms and molecules*; International Series of Monographs on Chemistry; Oxford university press, 1994; Vol. 16.

(4) Perdew, J. P.; Schmidt, K. Jacob's ladder of density functional approximations for the exchange-correlation energy. *AIP Conference Proceedings* **2001**, *577*, 1–20.

(5) Runge, E.; Gross, E. K. U. Density-Functional Theory for Time-Dependent Systems. *Phys. Rev. Lett.* **1984**, *52*, 997–1000.

(6) Shao, Y.; Head-Gordon, M.; Krylov, A. I. The spin-flip approach within time-dependent density functional theory: Theory and applications to diradicals. *J. Chem. Phys.* **2003**, *118*, 4807–4818.

(7) Gavnholt, J.; Olsen, T.; Engelund, M.; Schiøtz, J. Δ self-consistent field method to obtain potential energy surfaces of excited molecules on surfaces. *Phys. Rev. B* **2008**, *78*, 075441.

(8) Kowalczyk, T.; Tsuchimochi, T.; Chen, P.-T.; Top, L.; Van Voorhis, T. Excitation energies and Stokes shifts from a restricted open-shell Kohn–Sham approach. *J. Chem. Phys.* **2013**, *138*, 164101.

(9) Perdew, J. P.; Zunger, A. Self-interaction correction to density-functional approximations for many-electron systems. *Phys. Rev. B* **1981**, *23*, 5048–5079.

(10) Dreuw, A.; Head-Gordon, M. Failure of Time-Dependent Density Functional Theory for Long-Range Charge-Transfer Excited States: The Zincbacteriochlorin–Bacteriochlorin and Bacteriochlorophyll-Spheroidene Complexes. *J. Am. Chem. Soc.* **2004**, *126*, 4007–4016.

(11) Dreuw, A.; Head-Gordon, M. Single-Reference *ab initio* Methods for the Calculation of Excited States of Large Molecules. *Chem. Rev.* **2005**, *105*, 4009–4037.

(12) Vydrov, O. A.; Scuseria, G. E. Ionization potentials and electron affinities in the Perdew–Zunger self-interaction corrected density-functional theory. *J. Chem. Phys.* **2005**, *122*, 184107.

(13) Medvedev, M. G.; Bushmarinov, I. S.; Sun, J.; Perdew, J. P.; Lyssenko, K. A. Density functional theory is straying from the path toward the exact functional. *Science* **2017**, *355*, 49–52.

(14) Brorsen, K. R.; Yang, Y.; Pak, M. V.; Hammes-Schiffer, S. Is the Accuracy of Density Functional Theory for Atomization Energies and Densities in Bonding Regions Correlated? *J. Phys. Chem. Lett.* **2017**, *8*, 2076–2081.

(15) Hait, D.; Head-Gordon, M. How Accurate Is Density Functional Theory at Predicting Dipole Moments? An Assessment Using a New Database of 200 Benchmark Values. *J. Chem. Theory Comput.* **2018**, *14*, 1969–1981.

(16) Hait, D.; Head-Gordon, M. Communication: xDH double hybrid functionals can be qualitatively incorrect for non-equilibrium geometries: Dipole moment inversion and barriers to radical-radical association using XYG3 and XYGJ-OS. *J. Chem. Phys.* **2018**, *148*, 171102.

(17) Bao, J. L.; Gagliardi, L.; Truhlar, D. G. Self-Interaction Error in Density Functional Theory: An Appraisal. *J. Phys. Chem. Lett.* **2018**, *9*, 2353–2358.

(18) Polo, V.; Kraka, E.; Cremer, D. Electron correlation and the self-interaction error of density functional theory. *Mol. Phys.* **2002**, *100*, 1771–1790.

(19) Ciofini, I.; Adamo, C.; Chermette, H. Self-interaction error in density functional theory: a mean-field correction for molecules and large systems. *Chem. Phys.* **2005**, *309*, 67–76.

(20) Wu, Q.; Van Voorhis, T. Direct Calculation of Electron Transfer Parameters through Constrained Density Functional Theory. *J. Phys. Chem. A* **2006**, *110*, 9212–9218.

(21) Park, Y. C.; Senn, F.; Krykunov, M.; Ziegler, T. Self-Consistent Constricted Variational Theory RSCF-CV(∞)-DFT and Its Restrictions To Obtain a Numerically Stable ΔSCF-DFT-like Method: Theory and Calculations for Triplet States. *J. Chem. Theory Comput.* **2016**, *12*, 5438–5452.

(22) Tao, J.; Perdew, J. P.; Staroverov, V. N.; Scuseria, G. E. Climbing the Density Functional Ladder: Nonempirical Meta–Generalized Gradient Approximation Designed for Molecules and Solids. *Phys. Rev. Lett.* **2003**, *91*, 146401.

(23) Sun, J.; Ruzsinszky, A.; Perdew, J. P. Strongly Constrained and Appropriately Normed Semilocal Density Functional. *Phys. Rev. Lett.* **2015**, *115*, 036402.

(24) Zhao, Y.; Truhlar, D. G. A new local density functional for main-group thermochemistry, transition metal bonding, thermochemical kinetics, and noncovalent interactions. *J. Chem. Phys.* **2006**, *125*, 194101.

(25) Zhao, Y.; Truhlar, D. G. The M06 suite of density functionals for main group thermochemistry, thermochemical kinetics, noncovalent interactions, excited states, and transition elements: two new functionals and systematic testing of four M06-class functionals and 12 other functionals. *Theor. Chem. Acc.* **2008**, *120*, 215–241.

(26) Yanai, T.; Tew, D. P.; Handy, N. C. A new hybrid exchange-correlation functional using the Coulomb-attenuating method (CAM-B3LYP). *Chem. Phys. Lett.* **2004**, *393*, 51–57.

(27) Jin, Y.; Bartlett, R. J. The QTP family of consistent functionals and potentials in Kohn–Sham density functional theory. *J. Chem. Phys.* **2016**, *145*, 034107.

(28) Mardirossian, N.; Head-Gordon, M. ωB97X-V: A 10-parameter, range-separated hybrid, generalized gradient approximation density functional with nonlocal correlation, designed by a survival-of-the-fittest strategy. *Phys. Chem. Chem. Phys.* **2014**, *16*, 9904–9924.

(29) Mardirossian, N.; Head-Gordon, M. "ωB97M-V: A combinatorially optimized, range-separated hybrid, meta-GGA density functional with VV10 nonlocal correlation. *J. Chem. Phys.* **2016**, *144*, 214110.

(30) Vydrov, O. A.; Scuseria, G. E. Assessment of a long-range corrected hybrid functional. *J. Chem. Phys.* **2006**, *125*, 234109.

(31) Rohrdanz, M. A.; Herbert, J. M. Simultaneous benchmarking of ground- and excited-state properties with long-range-corrected density functional theory. *J. Chem. Phys.* **2008**, *129*, 034107.

(32) Vydrov, O. A.; Heyd, J.; Krukau, A. V.; Scuseria, G. E. Importance of short-range versus long-range Hartree–Fock exchange for the performance of hybrid density functionals. *J. Chem. Phys.* **2006**, *125*, 074106.

(33) Rohrdanz, M. A.; Martins, K. M.; Herbert, J. M. A long-range-corrected density functional that performs well for both ground-state properties and time-dependent density functional theory excitation energies, including charge-transfer excited states. *J. Chem. Phys.* **2009**, *130*, 054112.

(34) Livshits, E.; Baer, R. A well-tempered density functional theory of electrons in molecules. *Phys. Chem. Chem. Phys.* **2007**, *9*, 2932–2941.

(35) Salzner, U.; Aydin, A. Improved Prediction of Properties of π-Conjugated Oligomers with Range-Separated Hybrid Density Functionals. *J. Chem. Theory Comput.* **2011**, *7*, 2568–2583.

(36) Körzdörfer, T.; Parrish, R. M.; Marom, N.; Sears, J. S.; Sherrill, C. D.; Brédas, J.-L. Assessment of the performance of tuned range-separated hybrid density functionals in predicting accurate quasiparticle spectra. *Phys. Rev. B* **2012**, *86*, 205110.

(37) Stein, T.; Kronik, L.; Baer, R. Reliable Prediction of Charge Transfer Excitations in Molecular Complexes Using Time-Dependent Density Functional Theory. *J. Am. Chem. Soc.* **2009**, *131*, 2818–2820.

(38) Baer, R.; Livshits, E.; Salzner, U. Tuned range-separated hybrids in density functional theory. *Annu. Rev. Phys. Chem.* **2010**, *61*, 85–109.

(39) Iikura, H.; Tsuneda, T.; Yanai, T.; Hirao, K. A long-range correction scheme for generalized-gradient-approximation exchange functionals. *J. Chem. Phys.* **2001**, *115*, 3540–3544.

(40) Koopmans, T. Úber die Zuordnung von Wellenfunktionen und Eigenwerten zu den Einzelnen Elektronen Eines Atoms. *Physica* **1934**, *1*, 104–113.

(41) Livshits, E.; Granot, R. S.; Baer, R. A Density Functional Theory for Studying Ionization Processes in Water Clusters. *J. Phys. Chem. A* **2011**, *115*, 5735–5744.

(42) Sears, J. S.; Körzdörfer, T.; Zhang, C.-R.; Brédas, J.-L. Communication: Orbital instabilities and triplet states from time-dependent density functional theory and long-range corrected functionals. *J. Chem. Phys.* **2011**, *135*, 151103.

(43) Refaely-Abramson, S.; Baer, R.; Kronik, L. Fundamental and excitation gaps in molecules of relevance for organic photovoltaics from an optimally tuned range-separated hybrid functional. *Phys. Rev. B* **2011**, *84*, 075144.

(44) Kuritz, N.; Stein, T.; Baer, R.; Kronik, L. Charge-Transfer-Like $\pi \rightarrow \pi^*$ Excitations in Time-Dependent Density Functional Theory: A Conundrum and Its Solution. *J. Chem. Theory Comput.* **2011**, *7*, 2408–2415.

(45) Kronik, L.; Stein, T.; Refaely-Abramson, S.; Baer, R. Excitation Gaps of Finite-Sized Systems from Optimally Tuned Range-Separated Hybrid Functionals. *J. Chem. Theory Comput.* **2012**, *8*, 1515–1531.

(46) Körzdörfer, T.; Brédas, J.-L. Organic Electronic Materials: Recent Advances in the DFT Description of the Ground and Excited States Using Tuned Range-Separated Hybrid Functionals. *Acc. Chem. Res.* **2014**, *47*, 3284–3291.

(47) Jacquemin, D.; Moore, B.; Planchat, A.; Adamo, C.; Autschbach, J. Performance of an Optimally Tuned Range-Separated Hybrid Functional for 0–0 Electronic Excitation Energies. *J. Chem. Theory Comput.* **2014**, *10*, 1677–1685.

(48) Manna, A. K.; Refaely-Abramson, S.; Reilly, A. M.; Tkatchenko, A.; Neaton, J. B.; Kronik, L. Quantitative Prediction of Optical Absorption in Molecular Solids from an Optimally Tuned Screened Range-Separated Hybrid Functional. *J. Chem. Theory Comput.* **2018**, *14*, 2919–2929.

(49) Görling, A. Symmetry in density-functional theory. *Phys. Rev. A* **1993**, *47*, 2783–2799.

(50) Pople, J. A.; Nesbet, R. K. Self-Consistent Orbitals for Radicals. *J. Chem. Phys.* **1954**, *22*, 571–572.

(51) McWeeny, R. *Methods of molecular quantum mechanics*; Academic press, 1992.

(52) Marques, M.; Gross, E. Time-Dependent Density Functional Theory. *Annu. Rev. Phys. Chem.* **2004**, *55*, 427–455.

(53) Jensen, F. *Introduction to computational chemistry*; John Wiley & Sons, 2017.

(54) Baer, R.; Neuhauser, D. Density Functional Theory with Correct Long-Range Asymptotic Behavior. *Phys. Rev. Lett.* **2005**, *94*, 043002.

(55) Toulouse, J.; Colonna, F.; Savin, A. Long-range–short-range separation of the electron-electron interaction in density-functional theory. *Phys. Rev. A* **2004**, *70*, 062505.

(56) Chai, J.-D.; Head-Gordon, M. Systematic optimization of long-range corrected hybrid density functionals. *J. Chem. Phys.* **2008**, *128*, 084106.

(57) Szabo, A.; Ostlund, N. S. *Modern quantum chemistry: introduction to advanced electronic structure theory*; Courier Corporation, 2012.

(58) Abramowitz, M.; Stegun, I. A. *Handbook of mathematical functions: with formulas, graphs, and mathematical tables*; Courier Corporation, 1964; Vol. 55.

(59) Mori-Sánchez, P.; Cohen, A. J.; Yang, W. Localization and Delocalization Errors in Density Functional Theory and Implications for Band-Gap Prediction. *Phys. Rev. Lett.* **2008**, *100*, 146401.

(60) Becke, A. D. Density-functional exchange-energy approximation with correct asymptotic behavior. *Phys. Rev. A* **1988**, *38*, 3098–3100.

(61) Langreth, D. C.; Mehl, M. J. Beyond the local-density approximation in calculations of ground-state electronic properties. *Phys. Rev. B* **1983**, *28*, 1809–1834.

(62) Perdew, J. P.; Chevary, J. A.; Vosko, S. H.; Jackson, K. A.; Pederson, M. R.; Singh, D. J.; Fiolhais, C. Atoms, molecules, solids, and surfaces: Applications of the generalized gradient approximation for exchange and correlation. *Phys. Rev. B* **1992**, *46*, 6671–6687.

(63) Perdew, J. P.; Burke, K.; Ernzerhof, M. Generalized Gradient Approximation Made Simple. *Phys. Rev. Lett.* **1996**, *77*, 3865–3868.

(64) Murov, S. L.; Carmichael, I.; Hug, G. L. *Handbook of photochemistry*; CRC Press, 1993.

(65) Doering, J. P. Low-Energy Electron – Impact Study of the First, Second, and Third Triplet States of Benzene. *J. Chem. Phys.* **1969**, *51*, 2866–2870.

(66) Bolovinos, A.; Tsekeris, P.; Philis, J.; Pantos, E.; Andritsopoulos, G. Absolute vacuum ultraviolet absorption spectra of some gaseous azabenzenes. *J. Mol. Spect.* **1984**, *103*, 240–256.

(67) Hellner, L.; Vermeil, C. VUV excitation of benzene. *J. Mol. Spect.* **1976**, *60*, 71–92.

(68) Clar, E. Absorption spectra of aromatic hydrocarbons at low temperatures. LV-Aromatic hydrocarbons. *Spectrochim. Acta* **1950**, *4*, 116–121.

(69) Allan, M. Study of triplet states and short-lived negative ions by means of electron impact spectroscopy. *J. Electron Spectrosc. Relat. Phenom.* **1989**, *48*, 219–351.

(70) McClure, D. S. Excited Triplet States of Some Polyatomic Molecules. I. *J. Chem. Phys.* **1951**, *19*, 670–675.

(71) McClure, D. S. Triplet–Singlet Transitions in Organic Molecules. Lifetime Measurements of the Triplet State. *J. Chem. Phys.* **1949**, *17*, 905–913.

(72) Morgan, D. D.; Warshawsky, D.; Atkinson, T. The Relationship between Carcinogenic Activities of Polycyclic Aromatic Hydrocarbons and Their Singlet, Triplet and Singlet–Triplet Splitting Energies and Phosphorescence Lifetimes. *Photochem. Photobiol.* **1977**, *25*, 31–38.

(73) Moodie, M. M.; Reid, C. Inter- and Intramolecular Energy Transfer Processes. 3. Phosphorescence Bands of Some Carcinogenic Aromatic Hydrocarbons. *J. Chem. Phys.* **1954**, *22*, 252–254.

(74) McGlynn, S. P.; Azumi, T.; Kasha, M. External Heavy-Atom Spin–Orbital Coupling Effect. V. Absorption Studies of Triplet States. *J. Chem. Phys.* **1964**, *40*, 507–515.

(75) Perkampus, H.-H. *UV-VIS atlas of organic compounds*; VCH, 1992.

(76) Birks, J. B. *Photophysics of aromatic molecules*; Wiley monographs in chemical physics; John Wiley & Sons Ltd, 1970.

(77) Angliker, H.; Rommel, E.; Wirz, J. Electronic spectra of hexacene in solution (ground state, triplet state, dication and dianion). *Chem. Phys. Lett.* **1982**, *87*, 208–212.

(78) Clarke, R. H.; Hochstrasser, R. M. Location and assignment of the lowest triplet state of perylene. *J. Mol. Spect.* **1969**, *32*, 309–319.

(79) Paris, J. P.; Hirt, R. C.; Schmitt, R. G. Observed Phosphorescence and Singlet–Triplet Absorption in s-Triazine and Trimethyl-s-Triazine. *J. Chem. Phys.* **1961**, *34*, 1851–1852.

(80) Duncan, M. A.; Dietz, T. G.; Smalley, R. E. Two-color photoionization of naphthalene and benzene at threshold. *J. Chem. Phys.* **1981**, *75*, 2118–2125.

(81) Jalbout, A. F.; Trzaskowski, B.; Chen, E. C. M.; Chen, E. S.; Adamowicz, L. Electron affinities, gas phase acidities, and potential energy curves: Benzene. *Int. J. Quant. Chem.* **2007**, *107*, 1115–1125.

(82) Lyapustina, S. A.; Xu, S.; Nilles, J. M.; Bowen Jr., K. H. Solvent-induced stabilization of the naphthalene anion by water molecules: A negative cluster ion photoelectron spectroscopic study. *J. Chem. Phys.* **2000**, *112*, 6643–6648.

(83) Schäfer, W.; Schweig, A.; Vermeer, H.; Bickelhaupt, F.; Graaf, H. D. On the nature of the "free electron pair" on phosphorus in aromatic phosphorus compounds: The photoelectron spectrum of 2-phosphanaphthalene. *J. Electron Spectrosc. Relat. Phenom.* **1975**, *6*, 91–98.

(84) Ando, N.; Mitsui, M.; Nakajima, A. Comprehensive photoelectron spectroscopic study of anionic clusters of anthracene and its alkyl derivatives: Electronic structures bridging molecules to bulk. *J. Chem. Phys.* **2007**, *127*, 234305.

(85) Eland, J. Photoelectron spectra and ionization potentials of aromatic hydrocarbons. *Int. J. Mass Spectrom. Ion Phys.* **1972**, *9*, 214–219.

(86) Becker, R. S.; Chen, E. Extension of Electron Affinities and Ionization Potentials of Aromatic Hydrocarbons. *J. Chem. Phys.* **1966**, *45*, 2403–2410.

(87) Schmidt, W. Photoelectron spectra of polynuclear aromatics. V. Correlations with ultraviolet absorption spectra in the catacondensed series. *J. Chem. Phys.* **1977**, *66*, 828–845.

(88) Hager, J. W.; Wallace, S. C. Two-laser photoionization supersonic jet mass spectrometry of aromatic molecules. *Anal. Chem.* **1988**, *60*, 5–10.

(89) Mitsui, M.; Ando, N.; Nakajima, A. Mass Spectrometry and Photoelectron Spectroscopy of Tetracene Cluster Anions, $(\text{Tetracene})_n^-$ $(n = 1 - 100)$: Evidence for the Highly Localized Nature of Polarization in a Cluster Analogue of Oligoacene Crystals. *J. Phys. Chem. A* **2007**, *111*, 9644–9648.

(90) Stahl, D.; Maquin, F. Charge-stripping mass spectrometry of molecular ions from polyacenes and molecular orbital theory. *Chem. Phys. Lett.* **1984**, *108*, 613–617.

(91) Crocker, L.; Wang, T.; Kebarle, P. Electron affinities of some polycyclic aromatic hydrocarbons, obtained from electron-transfer equilibria. *J. Am. Chem. Soc.* **1993**, *115*, 7818–7822.

(92) Schiedt, J.; Weinkauf, R. Photodetachment photoelectron spectroscopy of perylene and CS_2: two extreme cases. *J. Chem. Phys.* **1997**, *274*, 18–22.

(93) Shchuka, M. I.; Motyka, A. L.; Topp, M. R. Two-photon threshold ionization spectroscopy of perylene and van der Waals complexes. *J. Chem. Phys.* **1989**, *164*, 87–95.

(94) Boschi, R.; Clar, E.; Schmidt, W. Photoelectron spectra of polynuclear aromatics. III. The effect of nonplanarity in sterically overcrowded aromatic hydrocarbons. *J. Chem. Phys.* **1974**, *60*, 4406–4418.

(95) Clar, E.; Robertson, J. M.; Schloegl, R.; Schmidt, W. Photoelectron spectra of polynuclear aromatics. 6. Applications to structural elucidation: "circumanthracene". *J. Am. Chem. Soc.* **1981**, *103*, 1320–1328.

(96) Hajgató, B.; Deleuze, M. S.; Tozer, D. J.; Proft, F. D. A benchmark theoretical study of the electron affinities of benzene and linear acenes. *J. Chem. Phys.* **2008**, *129*, 084308.

(97) Obenland, S.; Schmidt, W. Photoelectron spectra of polynuclear aromatics. IV. Helicenes. *J. Am. Chem. Soc.* **1975**, *97*, 6633–6638.

(98) Hung, R. R.; Grabowski, J. J. A precise determination of the triplet energy of carbon (C_{60}) by photoacoustic calorimetry. *J. Phys. Chem.* **1991**, *95*, 6073–6075.

(99) Arbogast, J. W.; Darmanyan, A. P.; Foote, C. S.; Diederich, F. N.; Whetten, R. L.; Rubin, Y.; Alvarez, M. M.; Anz, S. J. Photophysical properties of sixty atom carbon molecule (C_{60}). *J. Phys. Chem.* **1991**, *95*, 11–12.

(100) McVie, J.; Sinclair, R. S.; Truscott, T. G. Triplet states of copper and metal-free phthalocyanines. *J. Chem. Soc., Faraday Trans. 2* **1978**, *74*, 1870–1879.

(101) Gouterman, M.; Khalil, G.-E. Porphyrin free base phosphorescence. *J. Mol. Spect.* **1974**, *53*, 88–100.

(102) Vincett, P. S.; Voigt, E. M.; Rieckhoff, K. E. Phosphorescence and Fluorescence of Phthalocyanines. *J. Chem. Phys.* **1971**, *55*, 4131–4140.

(103) Petruska, J. Changes in the Electronic Transitions of Aromatic Hydrocarbons on Chemical Substitution. II. Application of Perturbation Theory to Substituted-Benzene Spectra. *J. Chem. Phys.* **1961**, *34*, 1120–1136.

(104) Palummo, M.; Hogan, C.; Sottile, F.; Bagalá, P.; Rubio, A. *Ab initio* electronic and optical spectra of free-base porphyrins: The role of electronic correlation. *J. Chem. Phys.* **2009**, *131*, 084102.

(105) Dvorak, M.; Müller, M.; Knoblauch, T.; Bünermann, O.; Rydlo, A.; Minniberger, S.; Harbich, W.; Stienkemeier, F. Spectroscopy of 3, 4, 9, 10-perylenetetracarboxylic dianhydride (PTCDA) attached to rare gas samples: Clusters vs. bulk matrices. I. Absorption spectroscopy. *J. Chem. Phys.* **2012**, *137*, 164301.

(106) Becker, R. S.; Seixas de Melo, J.; Maçanita, A. L.; Elisei, F. Comprehensive Evaluation of the Absorption, Photophysical, Energy Transfer, Structural, and Theoretical Properties of α-Oligothiophenes with One to Seven Rings. *J. Phys. Chem.* **1996**, *100*, 18683–18695.

(107) Seixas de Melo, J.; Silva, L. M.; Arnaut, L. G.; Becker, R. S. Singlet and triplet energies of α-oligothiophenes: A spectroscopic, theoretical, and photoacoustic study: Extrapolation to polythiophene. *J. Chem. Phys.* **1999**, *111*, 5427–5433.

(108) Shizuka, H.; Ueki, Y.; Iizuka, T.; Kanamaru, N. Radiative and radiationless transitions in the excited state of methyl- and methylene-substituted benzenes in condensed media. *J. Phys. Chem.* **1982**, *86*, 3327–3333.

(109) Marchetti, A. P.; Kearns, D. R. Investigation of Singlet–Triplet Transitions by the Phosphorescence Excitation Method. IV. The Singlet–Triplet Absorption Spectra of Aromatic Hydrocarbons. *J. Am. Chem. Soc.* **1967**, *89*, 768–777.

(110) Kearns, D. R.; Case, W. A. Investigation of Singlet $\rightarrow$ Triplet Transitions by the Phosphorescence Excitation Method. III. Aromatic Ketones and Aldehydes. *J. Am. Chem. Soc.* **1966**, *88*, 5087–5097.

(111) Ghoshal, S. K.; Sarkar, S. K.; Kastha, G. S. Effects of Intermolecular Hydrogen-bonding on the Luminescence Properties of Acetophenone, Characterization of Emission States. *Bull. Chem. Soc. Jpn.* **1981**, *54*, 3556–3561.

(112) Kuboyama, A.; Yabe, S. Phosphorescence bands of quinones and α-diketones. *Bull. Chem. Soc. Jpn.* **1967**, *40*, 2475–2479.

(113) Borkman, R. F.; Kearns, D. R. Heavy-Atom and Substituent Effects on $S - T$ Transitions of Halogenated Carbonyl Compounds. *J. Chem. Phys.* **1967**, *46*, 2333–2341.

(114) Kanda, Y.; Shimada, R.; Sakai, Y. The phosphorescence spectrum of biphenyl at 90 °K. *Spectrochim. Acta* **1961**, *17*, 1–6.

(115) Berlman, I. B. *Handbook of Fluorescence Spectra of Aromatic Molecules*, 2nd ed.; Academic Press, 1971.

(116) Lim, E. C.; Li, Y. H. Luminescence of Biphenyl and Geometry of the Molecule in Excited Electronic States. *J. Chem. Phys.* **1970**, *52*, 6416–6422.

(117) Bulliard, C.; Allan, M.; Wirtz, G.; Haselbach, E.; Zachariasse, K. A.; Detzer, N.; Grimme, S. Electron Energy Loss and DFT/SCI Study of the Singlet and Triplet Excited States of Aminobenzonitriles and Benzoquinuclidines: Role of the Amino Group Twist Angle. *J. Phys. Chem. A* **1999**, *103*, 7766–7772.

(118) Adams, J. E.; Mantulin, W. W.; Huber, J. R. Effect of molecular geometry on spin–orbit coupling of aromatic amines in solution. Diphenylamine, iminobibenzyl, acridan, and carbazole. *J. Am. Chem. Soc.* **1973**, *95*, 5477–5481.

(119) Grimme, S.; Waletzke, M. A combination of Kohn–Sham density functional theory and multi-reference configuration interaction methods. *J. Chem. Phys.* **1999**, *111*, 5645–5655.

(120) Carsey, T. P.; Findley, G. L.; McGlynn, S. P. Systematics in the electronic spectra of polar molecules. 1. $Para$-disubstituted benzenes. *J. Am. Chem. Soc.* **1979**, *101*, 4502–4510.

(121) Fujitsuka, M.; Sato, T.; Sezaki, F.; Tanaka, K.; Watanabe, A.; Ito, O. Laser flash photolysis study on the photoinduced reactions of 3,3′-bridged bithiophenes. *J. Chem. Soc., Faraday Trans.* **1998**, *94*, 3331–3337.

(122) Wasserberg, D.; Marsal, P.; Meskers, S. C. J.; Janssen, R. A. J.; Beljonne, D. Phosphorescence and Triplet State Energies of Oligothiophenes. *J. Phys. Chem. B* **2005**, *109*, 4410–4415.

(123) Dyck, R. H.; McClure, D. S. Ultraviolet Spectra of Stilbene, p-Monohalogen Stilbenes, and Azobenzene and the $trans$ to cis Photoisomerization Process. *J. Chem. Phys.* **1962**, *36*, 2326–2345.

(124) Saltiel, J.; Khalil, G.-E.; Schanze, K. $Trans$-stilbene phosphorescence. *Chem. Phys. Lett.* **1980**, *70*, 233–235.

(125) Beljonne, D.; Cornil, J.; Friend, R. H.; Janssen, R. A. J.; Brédas, J. L. Influence of Chain Length and Derivatization on the Lowest Singlet and Triplet States and Intersystem Crossing in Oligothiophenes. *J. Am. Chem. Soc.* **1996**, *118*, 6453–6461.

(126) Scaiano, J. C.; Redmond, R. W.; Mehta, B.; Arnason, J. T. Efficiency of the Photoprocesses Leading to Singlet Oxygen ($^1\Delta_g$) Generation by α-Terthinenyl: Optical Absorption, Optoacoustic Calorimetry and Infrared Luminescence Studies. *Photochem. Photobiol.* **1990**, *52*, 655–659.

(127) Burke, F. P.; Small, G. J.; Braun, J. R.; Lin, T.-S. The polarized absorption, fluorescence and phosphorescence spectra of 1,3-diazaazulene. *Chem. Phys. Lett.* **1973**, *19*, 574–579.

(128) Herkstroeter, W. G. Triplet energies of azulene, β-carotene, and ferrocene. *J. Am. Chem. Soc.* **1975**, *97*, 4161–4167.

(129) Tway, P. C.; Love, L. J. C. Photophysical properties of benzimidazole and thiabendazole and their homologs. Effect of substituents and solvent on the nature of the transition. *J. Phys. Chem.* **1982**, *86*, 5223–5226.

(130) Zander, M. Zur Photolumineszenz von Benzologen des Thiophens. *Z. Naturforsch.* **1985**, *40A*, 497–502.

(131) Goodman, L.; Harrell, R. W. Calculation of $n \rightarrow \pi^\star$ Transition Energies in N-Heterocyclic Molecules by a One-Electron Approximation. *J. Chem. Phys.* **1959**, *30*, 1131–1138.

(132) Wintgens, V.; Valat, P.; Kossanyi, J.; Biczok, L.; Demeter, A.; Berces, T. Spectroscopic properties of aromatic dicarboximides. Part 1.-N-H and N-methyl-substituted naphthalimides. *J. Chem. Soc., Faraday Trans.* **1994**, *90*, 411–421.

(133) Evans, D. F. Magnetic perturbation of singlet–triplet transitions. Part III. Benzene derivatives and heterocyclic compounds. *J. Chem. Soc.* **1959**, 2753–2757.

(134) Najbar, J.; Trzcinska, B. M.; Urbanek, Z. H.; Proniewicz, L. M. *Acta Phys. Pol., A* **1980**, *A58*, 331–344.

(135) Suga, K.; Kinoshita, M. Static and Dynamic Properties of Quinoxalines in the Phosphorescent Triplet State from Optically Detected Magnetic Resonance. *Bull. Chem. Soc. Jpn.* **1982**, *55*, 1695–1704.

(136) Anderson, J. L.; An, Y.-Z.; Rubin, Y.; Foote, C. S. Photophysical Characterization and Singlet Oxygen Yield of a Dihydrofullerene. *J. Am. Chem. Soc.* **1994**, *116*, 9763–9764.

(137) Johnstone, R. A. W.; Mellon, F. A. Photoelectron spectroscopy of sulphur-containing heteroaromatics and molecular orbital calculations. *J. Chem. Soc., Faraday Trans. 2* **1973**, *69*, 1155–1163.

(138) Eland, J. Photoelectron spectra of conjugated hydrocarbons and heteromolecules. *Int. J. Mass Spectrom. Ion Phys.* **1969**, *2*, 471–484.

(139) Muigg, D.; Scheier, P.; Becker, K.; Märk, T. D. Measured appearance energies of C_n^+ ($3 \leq n \leq 10$) fragment ions produced by electron impact on C_{60}. *J. Phys. B* **1996**, *29*, 5193–5198.

(140) Huang, D.-L.; Dau, P. D.; Liu, H.-T.; Wang, L.-S. High-resolution photoelectron imaging of cold C_{60} anions and accurate determination of the electron affinity of C_{60}. *J. Chem. Phys.* **2014**, *140*, 224315.

(141) Dewar, M. J. S.; Haselbach, E.; Worley, S. D. Calculated and Observed Ionization Potentials of Unsaturated Polycyclic Hydrocarbons; Calculated Heats of Formation by Several Semiempirical S.C.F. M.O. Methods. *Proceedings of the Royal Society of London A: Mathematical, Physical and Engineering Sciences* **1970**, *315*, 431–442.

(142) Wojnárovits, L.; Földiák, G. Electron-capture detection of aromatic hydrocarbons. *J. Chromatogr. A* **1981**, *206*, 511–519.

(143) Eley, D. D.; Hazeldine, D. J.; Palmer, T. F. Mass spectra, ionisation potentials and related properties of metal-free and transition metal phthalocyanines. *J. Chem. Soc., Faraday Trans. 2* **1973**, *69*, 1808–1814.

(144) Khandelwal, S. C.; Roebber, J. L. The photoelectron spectra of tetraphenylporphine and some metallotetraphenylporphyrins. *Chem. Phys. Lett.* **1975**, *34*, 355–359.

(145) Butler, J. J.; Baer, T. Thermochemistry and dissociation dynamics of state selected C_4H_4X ions. 1. Thiophene. *J. Am. Chem. Soc.* **1980**, *102*, 6764–6769.

(146) Hunter, E. P. L.; Lias, S. G. Evaluated Gas Phase Basicities and Proton Affinities of Molecules: An Update. *J. Phys. Chem. Ref. Data* **1998**, *27*, 413–656.

(147) Sato, N.; Seki, K.; Inokuchi, H. Polarization energies of organic solids determined by ultraviolet photoelectron spectroscopy. *J. Chem. Soc., Faraday Trans. 2* **1981**, *77*, 1621–1633.

(148) Chen, H. L.; Pan, Y. H.; Groh, S.; Hagan, T. E.; Ridge, D. P. Gas-phase charge-transfer reactions and electron affinities of macrocyclic, anionic nickel complexes: Ni(SALEN), Ni(tetraphenylporphyrin), and derivatives. *J. Am. Chem. Soc.* **1991**, *113*, 2766–2767.

(149) Pasinszki, T.; Krebsz, M.; Vass, G. Ground and ionic states of 1,2,5-thiadiazoles: An UV-photoelectron spectroscopic and theoretical study. *J. Mol. Spect.* **2010**, *966*, 85–91.

(150) Berkowitz, J. Photoelectron spectroscopy of phthalocyanine vapors. *J. Chem. Phys.* **1979**, *70*, 2819–2828.

(151) Stenuit, G.; Castellarin-Cudia, C.; Plekan, O.; Feyer, V.; Prince, K. C.; Goldoni, A.; Umari, P. Valence electronic properties of porphyrin derivatives. *Phys. Chem. Chem. Phys.* **2010**, *12*, 10812–10817.

(152) Dori, N.; Menon, M.; Kilian, L.; Sokolowski, M.; Kronik, L.; Umbach, E. Valence electronic structure of gas-phase 3,4,9,10-perylene tetracarboxylic acid dianhydride: Experiment and theory. *Phys. Rev. B* **2006**, *73*, 195208.

(153) Dallinga, J. W.; Nibbering, N. M. M.; Louter, G. J. Formation and structure of $[C_8H_8O]^+\cdot$ ions, generated from gas phase ions of phenyl-cyclopropylcarbinol and 1-phenyl-1-(hydroxymethyl)cyclopropane. *Org. Mass Spectrom.* **1981**, *16*, 183–187.

(154) Wentworth, W. E.; Kao, L. W.; Becker, R. S. Electron affinities of substituted aromatic compounds. *J. Phys. Chem.* **1975**, *79*, 1161–1169.

(155) Paul, G.; Kebarle, P. Electron affinities of cyclic unsaturated dicarbonyls: maleic anhydrides, maleimides, and cyclopentenedione. *J. Am. Chem. Soc.* **1989**, *111*, 464–470.

(156) Polevoi, A. V.; Matyuk, V. M.; Grigor'eva, G. A.; Potapov, V. K. Formation of intermediate products during the resonance stepwise polarization of dibenzyl ketone and benzil molecules. *High Energy Chem.(Engl. Transl.);(United States)* **1987**, *21*, 17–21.

(157) Grützmacher, H.-F.; Schubert, R. Substituent effects in the mass spectra of benzoyl hetarenes. *Org. Mass Spectrom.* **1979**, *14*, 567–570.

(158) Maeyama, T.; Yagi, I.; Fujii, A.; Mikami, N. Photoelectron spectroscopy of microsolvated benzophenone radical anions to reveal the origin of solvatochromic shifts in alcoholic media. *Chem. Phys. Lett.* **2008**, *457*, 18–22.

(159) Loudon, A. G.; Mazengo, R. Z. Steric strain and electron-impact. The behaviour of some n,n'-dimethyl-1,1-binaphthyls, some n,n'-dimethylbiphenyls and model compounds. *Org. Mass Spectrom.* **1974**, *8*, 179–187.

(160) Kobayashi, T. Conformational analysis of terphenyls by photoelectron spectroscopy. *Bull. Chem. Soc. Jpn.* **1983**, *56*, 3224–3229.

(161) Haink, H. J.; Adams, J. E.; Huber, J. R. The Electronic Structure of Aromatic Amines: Photoelectron Spectroscopy of Diphenylamine, Iminobibenzyl, Acridan and Carbazole. *Ber. Bunsen-Ges. Phys. Chem.* **1974**, *78*, 436–440.

(162) Debies, T. P.; Rabalais, J. W. Photoelectron spectra of substituted benzenes. III. Bonding with Group V substituents. *Inorg. Chem.* **1974**, *13*, 308–312.

(163) Potapov, V. K.; Sorokin, V. V. Photoionization and ion-molecule reactions in quinones and alcohols. *High Energy Chem.(Engl. Transl.);(United States)* **1971**, *5*, 435–487.

(164) Lipert, R. J.; Colson, S. D. Accurate ionization potentials of phenol and phenol-(H_2O) from the electric field dependence of the pump–probe photoionization threshold. *J. Chem. Phys.* **1990**, *92*, 3240–3241.

(165) Hudson, B. S.; Ridyard, J. N. A.; Diamond, J. Polyene spectroscopy. Photoelectron spectra of the diphenylpolyenes. *J. Am. Chem. Soc.* **1976**, *98*, 1126–1129.

(166) Siegert, S.; Vogeler, F.; Marian, C. M.; Weinkauf, R. Throwing light on dark states of α-oligothiophenes of chain lengths 2 to 6: radical anion photoelectron spectroscopy and excited-state theory. *Phys. Chem. Chem. Phys.* **2011**, *13*, 10350–10363.

(167) Lu, K. T.; Eiden, G. C.; Weisshaar, J. C. Toluene cation: nearly free rotation of the methyl group. *J. Phys. Chem.* **1992**, *96*, 9742–9748.

(168) Schiedt, J.; Knott, W. J.; Le Barbu, K.; Schlag, E. W.; Weinkauf, R. Microsolvation of similar-sized aromatic molecules: Photoelectron spectroscopy of bithiophene–, azulene–, and naphthalene–water anion clusters. *J. Chem. Phys.* **2000**, *113*, 9470–9478.

(169) Jochims, H. W.; Rasekh, H.; Rühl, E.; Baumgärtel, H.; Leach, S. The photofragmentation of naphthalene and azulene monocations in the energy range 7–22 eV. *Chem. Phys.* **1992**, *168*, 159–184.

(170) Klasinc, L.; Trinajstića, N.; Knop, J. V. Application of photoelectron spectroscopy to biologically active molecules and their constituent parts. VIII. Thalidomide. *Int. J. Quant. Chem.* **1980**, *18*, 403–409.

(171) Ham, D. V. D.; Meer, D. V. D. The photoelectron spectra of the diazanaphthalenes. *Chem. Phys. Lett.* **1972**, *12*, 447–453.

(172) Dillow, G. W.; Kebarle, P. Electron affinities of aza-substituted polycyclic aromatic hydrocarbons. *Can. J. Chem.* **1989**, *67*, 1628–1631.

(173) Brogli, F.; Heilbronner, E.; Kobayashi, T. Photoelectron Spektra of Azabenzenes and Azanaphthalenes: II. A Reinvestigation of Azanaphthalenes by High-Resolution Photoelectron Spectroscopy. *Helv. Chim. Acta* **1972**, *55*, 274–288.

(174) Huang, S.; Zhang, Q.; Shiota, Y.; Nakagawa, T.; Kuwabara, K.; Yoshizawa, K.; Adachi, C. Computational Prediction for Singlet- and Triplet-Transition Energies of Charge-Transfer Compounds. *J. Chem. Theory Comput.* **2013**, *9*, 3872–3877.

(175) Lee, J.; Shizu, K.; Tanaka, H.; Nomura, H.; Yasuda, T.; Adachi, C. Oxadiazole- and triazole-based highly-efficient thermally activated delayed fluorescence emitters for organic light-emitting diodes. *J. Mater. Chem. C* **2013**, *1*, 4599–4604.

(176) Wu, S.; Aonuma, M.; Zhang, Q.; Huang, S.; Nakagawa, T.; Kuwabara, K.; Adachi, C. High-efficiency deep-blue organic light-emitting diodes based on a thermally activated delayed fluorescence emitter. *J. Mater. Chem. C* **2014**, *2*, 421–424.

(177) Zhang, Q.; Li, B.; Huang, S.; Nomura, H.; Tanaka, H.; Adachi, C. Efficient blue organic light-emitting diodes employing thermally activated delayed fluorescence. *Nat. Photon.* **2014**, *8*, 326–332.

(178) Hait, D.; Zhu, T.; McMahon, D. P.; Van Voorhis, T. Prediction of Excited-State Energies and Singlet–Triplet Gaps of Charge-Transfer States Using a Restricted Open-Shell Kohn–Sham Approach. *J. Chem. Theory Comput.* **2016**, *12*, 3353–3359.

(179) Longworth, J. W.; Rahn, R. O.; Shulman, R. G. Luminescence of Pyrimidines, Purines,

Nucleosides, and Nucleotides at 77 °K. The Effect of Ionization and Tautomerization. *J. Chem. Phys.* **1966**, *45*, 2930–2939.

(180) Daniels, M.; Hauswirth, W. Fluorescence of the Purine and Pyrimidine Bases of the Nucleic Acids in Neutral Aqueous Solution at 300 °K. *Science* **1971**, *171*, 675–677.

(181) Lin, J.; Yu, C.; Peng, S.; Akiyama, I.; Li, K.; Lee, L. K.; LeBreton, P. R. Ultraviolet photoelectron studies of the ground-state electronic structure and gas-phase tautomerism of purine and adenine. *J. Am. Chem. Soc.* **1980**, *102*, 4627–4631.

(182) Aflatooni, K.; Gallup, G. A.; Burrow, P. D. Electron Attachment Energies of the DNA Bases. *J. Phys. Chem. A* **1998**, *102*, 6205–6207.

(183) Guéron, M.; Eisinger, J.; Shulman, R. G. Excited States of Nucleotides and Singlet Energy Transfer in Polynucleotides. *J. Chem. Phys.* **1967**, *47*, 4077–4091.

(184) Nguyen, M. T.; Zhang, R.; Nam, P.-C.; Ceulemans, A. Singlet–Triplet Energy Gaps of Gas-Phase RNA and DNA Bases. A Quantum Chemical Study. *J. Phys. Chem. A* **2004**, *108*, 6554–6561.

(185) Li, X.; Bowen, K. H.; Haranczyk, M.; Bachorz, R. A.; Mazurkiewicz, K.; Rak, J.; Gutowski, M. Photoelectron spectroscopy of adiabatically bound valence anions of rare tautomers of the nucleic acid bases. *J. Chem. Phys.* **2007**, *127*, 174309.

(186) Schiedt, J.; Weinkauf, R.; Neumark, D. M.; Schlag, E. W. Anion spectroscopy of uracil, thymine and the amino-oxo and amino-hydroxy tautomers of cytosine and their water clusters. *Chem. Phys.* **1998**, *239*, 511–524.

(187) Dougherty, D.; Younathan, E.; Voll, R.; Abdulnur, S.; McGlynn, S. Photoelectron spectroscopy of some biological molecules. *J. Electron Spectrosc. Relat. Phenom.* **1978**, *13*, 379–393.

(188) Dougherty, D.; Wittel, K.; Meeks, J.; McGlynn, S. P. Photoelectron spectroscopy of carbonyls. Ureas, uracils, and thymine. *J. Am. Chem. Soc.* **1976**, *98*, 3815–3820.

(189) Hendricks, J. H.; Lyapustina, S. A.; de Clercq, H. L.; Snodgrass, J. T.; Bowen, K. H. Dipole bound, nucleic acid base anions studied via negative ion photoelectron spectroscopy. *J. Chem. Phys.* **1996**, *104*, 7788–7791.

(190) Yu, C.; O'Donnell, T. J.; LeBreton, P. R. Ultraviolet photoelectron studies of volatile nucleoside models. Vertical ionization potential measurements of methylated uridine, thymidine, cytidine, and adenosine. *J. Phys. Chem.* **1981**, *85*, 3851–3855.

(191) Kearns, D. R.; Marsh, G.; Schaffner, K. Investigation of singlet $\rightarrow$ triplet transitions by phosphorescence excitation spectroscopy. IX. Conjugated enones. *J. Am. Chem. Soc.* **1971**, *93*, 3129–3137.

(192) Dvornikov, S. S.; Knyukshto, V. N.; Solovev, K. N.; Tsvirko, M. P. Phosphorescence of chlorophyllis a and b and their pheophytins. *Opt. Spect. (USSR)* **1979**, *46*, 385–388.

(193) McLendon, G.; Miller, D. S. Metalloporphyrins catalyse the photo-reduction of water to H_2. *J. Chem. Soc., Chem. Commun.* **1980**, 533–534.

(194) Chattopadhyay, S. K.; Kumar, C. V.; Das, P. K. Triplet-state photophysics of retinal analogues. Interaction of polyene triplets with the di-t-butylnitroxy radical. *J. Chem. Soc., Faraday Trans. 1* **1984**, *80*, 1151–1161.

(195) Becker, R. S.; Inuzuka, K.; Balke, D. E. Spectroscopy and photochemistry of retinals. I. Theoretical and experimental considerations of absorption spectra. *J. Am. Chem. Soc.* **1971**, *93*, 38–42.

(196) Thomson, A. J. Fluorescence Spectra of Some Retinyl Polyenes. *J. Chem. Phys.* **1969**, *51*, 4106–4116.

(197) Haley, J. L.; Fitch, A. N.; Goyal, R.; Lambert, C.; Truscott, T. G.; Chacon, J. N.; Stirling, D.; Schalch, W. The S_1 and T_1 energy levels of all-$trans$-β-carotene. *J. Chem. Soc., Chem. Commun.* **1992**, 1175–1176.

(198) Chattopadhyay, S. K.; Kumar, C. V.; Das, P. K. Triplet Excitation Transfer Involving β-Ionone. A Kinetic Study by Laser Flash Photolysis. *Photochem. Photobiol.* **1985**, *42*, 17–24.

(199) Marsh, G.; Kearns, D. R.; Fisch, M. Investigation of singlet $\rightarrow$ triplet and singlet $\rightarrow$ singlet transitions by phosphorescence excitation spectroscopy. VIII. Santonins. *J. Am. Chem. Soc.* **1970**, *92*, 2252–2257.

(200) Hansen, P. E.; Undheim, K. Mass spectrometry of onium compounds. XXIX. Ionisation potential in structure analysis of valence isomers. *Acta Chem. Scand., Ser. B* **1975**, 221–223.

(201) Case, W. A.; Kearns, D. R. Investigation of S $\rightarrow$ T and S $\rightarrow$ S Transitions by Phosphorescence Excitation Spectroscopy VII. 1-Indanone and Other Aromatic Ketones. *J. Chem. Phys.* **1970**, *52*, 2175–2191.

(202) Matsushima, R.; Sakai, K. Specific photoreactions of flavanones typical of n,π^* and π,π^* characters in lowest triplet states. *J. Chem. Soc., Perkin Trans. 2* **1986**, 1217–1222.

(203) Bhattacharyya, K.; Das, P. K.; Ramamurthy, V.; Rao, V. P. Triplet-state photophysics and transient photochemistry of cyclic enethiones. A laser flash photolysis study. *J. Chem. Soc., Faraday Trans. 2* **1986**, *82*, 135–147.

(204) Mantulin, W. W.; Song, P.-S. Excited states of skin-sensitizing coumarins and psoralens. Spectroscopic studies. *J. Am. Chem. Soc.* **1973**, *95*, 5122–5129.

(205) Usacheva, M. N.; Osipov, V. V.; Drozdenko, I. V.; Dilung, I. *Russ. J. Phys. Chem.* **1984**, *58*, 1550–1553.

(206) Maier, J. P.; Muller, J.-F.; Kubota, T.; Yamakawa, M. Ionisation Energies and the Electronic Structures of the N-oxides of Azanaphthalenes and azaanthracenes. *Helv. Chim. Acta* **1975**, *58*, 1641–1648.

(207) Kokubo, S.; Ando, N.; Koyasu, K.; Mitsui, M.; Nakajima, A. Negative ion photoelectron spectroscopy of acridine molecular anion and its monohydrate. *J. Chem. Phys.* **2004**, *121*, 11112–11117.

(208) Chambers, R. W.; Kearns, D. R. Triplet States of Some Common Photosensitizing Dyes. *Photochem. Photobiol.* **1969**, *10*, 215–219.

(209) Korobov, V. E.; Chibisov, A. K. Primary Photoprocesses in Colorant Molecules. *Russ. Chem. Rev.* **1983**, *52*, 27.

(210) Sikorska, E.; Khmelinskii, I. V.; Prukała, W.; Williams, S. L.; Patel, M.; Worrall, D. R.; Bourdelande, J. L.; Koput, J.; Sikorski, M. Spectroscopy and Photophysics of Lumiflavins and Lumichromes. *J. Phys. Chem. A* **2004**, *108*, 1501–1508.

(211) Palmer, M. H.; Simpson, I.; Platenkamp, R. J. The electronic structure of flavin derivatives. *J. Mol. Struct.* **1980**, *66*, 243–263.

(212) Timoshenko, M. M.; Korkoshko, I. V.; Kleimenov, V. I.; Petrachenko, N. E.; Chizhov, I. V.; Rylkov, V. V.; Akopian, M. E. Ionization potentials of rhodamine dyes. *Dokl. Phys. Chem. (USSR)* **1981**, *260*, 138–140.

(213) Lee, C.; Yang, W.; Parr, R. G. Development of the Colle–Salvetti correlation-energy formula into a functional of the electron density. *Phys. Rev. B* **1988**, *37*, 785–789.

(214) Becke, A. D. A new mixing of Hartree–Fock and local density-functional theories. *J. Chem. Phys.* **1993**, *98*, 1372–1377.

(215) Kiefer, J. Sequential minimax search for a maximum. *Proc. Am. Math. Soc.* **1953**, *4*, 502–506.

(216) Press, W. H. *Numerical recipes 3rd edition: The art of scientific computing*; Cambridge university press, 2007.

(217) Hirata, S.; Head-Gordon, M. Time-dependent density functional theory within the Tamm–Dancoff approximation. *Chem. Phys. Lett.* **1999**, *314*, 291–299.

(218) Becke, A. D. Density-functional thermochemistry. III. The role of exact exchange. *J. Chem. Phys.* **1993**, *98*, 5648–5652.

(219) Adamo, C.; Barone, V. Toward reliable density functional methods without adjustable parameters: The PBE0 model. *J. Chem. Phys.* **1999**, *110*, 6158–6170.

(220) Dunning Jr., T. H. Gaussian basis sets for use in correlated molecular calculations. I. The atoms boron through neon and hydrogen. *J. Chem. Phys.* **1989**, *90*, 1007–1023.

(221) Shao, Y.; Gan, Z.; Epifanovsky, E.; Gilbert, A. T. B.; Wormit, M.; Kussmann, J.; Lange, A. W.; Behn, A.; Deng, J.; Feng, X.; Ghosh, D.; Goldey, M.; Horn, P. R.; Jacobson, L. D.; Kaliman, I.; Khaliullin, R. Z.; Kús, T.; Landau, A.; Liu, J.; Proynov, E. I.; Rhee, Y. M.; Richard, R. M.; Rohrdanz, M. A.; Steele, R. P.; Sundstrom, E. J.; Woodcock III, H. L.; Zimmerman, P. M.; Zuev, D.; Albrecht, B.; Alguire, E.; Austin, B.; Beran, G. J. O.; Bernard, Y. A.; Berquist, E.; Brandhorst, K.; Bravaya, K. B.; Brown, S. T.; Casanova, D.; Chang, C.-M.; Chen, Y.; Chien, S. H.; Closser, K. D.; Crittenden, D. L.; Diedenhofen, M.; DiStasio Jr., R. A.; Dop, H.; Dutoi, A. D.; Edgar, R. G.; Fatehi, S.; Fusti-Molnar, L.; Ghysels, A.; Golubeva-Zadorozhnaya, A.; Gomes, J.; Hanson-Heine, M. W. D.; Harbach, P. H. P.; Hauser, A. W.; Hohenstein, E. G.; Holden, Z. C.; Jagau, T.-C.; Ji, H.; Kaduk, B.; Khistyaev, K.; Kim, J.; Kim, J.; King, R. A.; Klunzinger, P.; Kosenkov, D.; Kowalczyk, T.; Krauter, C. M.; Lao, K. U.; Laurent, A.; Lawler, K. V.; Levchenko, S. V.; Lin, C. Y.; Liu, F.; Livshits, E.; Lochan, R. C.; Luenser, A.; Manohar, P.; Manzer, S. F.; Mao, S.-P.; Mardirossian, N.; Marenich, A. V.; Maurer, S. A.; Mayhall, N. J.; Oana, C. M.; Olivares-Amaya, R.; O'Neill, D. P.; Parkhill, J. A.; Perrine, T. M.; Peverati, R.; Pieniazek, P. A.;

Prociuk, A.; Rehn, D. R.; Rosta, E.; Russ, N. J.; Sergueev, N.; Sharada, S. M.; Sharmaa, S.; Small, D. W.; Sodt, A.; Stein, T.; Stück, D.; Su, Y.-C.; Thom, A. J. W.; Tsuchimochi, T.; Vogt, L.; Vydrov, O.; Wang, T.; Watson, M. A.; Wenzel, J.; White, A.; Williams, C. F.; Vanovschi, V.; Yeganeh, S.; Yost, S. R.; You, Z.-Q.; Zhang, I. Y.; Zhang, X.; Zhou, Y.; Brooks, B. R.; Chan, G. K. L.; Chipman, D. M.; Cramer, C. J.; Goddard III, W. A.; Gordon, M. S.; Hehre, W. J.; Klamt, A.; Schaefer III, H. F.; Schmidt, M. W.; Sherrill, C. D.; Truhlar, D. G.; Warshel, A.; Xua, X.; Aspuru-Guzik, A.; Baer, R.; Bell, A. T.; Besley, N. A.; Chai, J.-D.; Dreuw, A.; Dunietz, B. D.; Furlani, T. R.; Gwaltney, S. R.; Hsu, C.-P.; Jung, Y.; Kong, J.; Lambrecht, D. S.; Liang, W.; Ochsenfeld, C.; Rassolov, V. A.; Slipchenko, L. V.; Subotnik, J. E.; Van Voorhis, T.; Herbert, J. M.; Krylov, A. I.; Gill, P. M. W.; Head-Gordon, M. Advances in molecular quantum chemistry contained in the Q-Chem 4 program package. *Mol. Phys.* **2015**, *113*, 184–215.

(222) Tu, C.; Liang, W. NB-Type Electronic Asymmetric Compounds as Potential Blue-Color TADF Emitters: Steric Hindrance, Substitution Effect, and Electronic Characteristics. *ACS Omega* **2017**, *2*, 3098–3109.

(223) Liu, J.; Adamska, L.; Doorn, S. K.; Tretiak, S. Singlet and triplet excitons and charge polarons in cycloparaphenylenes: a density functional theory study. *Phys. Chem. Chem. Phys.* **2015**, *17*, 14613–14622.

(224) Zhang, Y.; Steyrleuthner, R.; Brédas, J.-L. Charge Delocalization in Oligomers of Poly(2,5-bis(3-alkylthiophene-2-yl)thieno[3,2-b]thiophene) (PBTTT). *J. Phys. Chem. C* **2016**, *120*, 9671–9677.

(225) Isborn, C. M.; Mar, B. D.; Curchod, B. F. E.; Tavernelli, I.; Martínez, T. J. The Charge Transfer Problem in Density Functional Theory Calculations of Aqueously Solvated Molecules. *J. Phys. Chem. B* **2013**, *117*, 12189–12201.

(226) Maitra, N. T.; Zhang, F.; Cave, R. J.; Burke, K. Double excitations within time-dependent density functional theory linear response. *J. Chem. Phys.* **2004**, *120*, 5932–5937.

(227) Maitra, N. T. Undoing static correlation: Long-range charge transfer in time-dependent density-functional theory. *J. Chem. Phys.* **2005**, *122*, 234104.

(228) Ullrich, C. A. Time-dependent density-functional theory beyond the adiabatic approximation: Insights from a two-electron model system. *J. Chem. Phys.* **2006**, *125*, 234108.

(229) Li Manni, G.; Carlson, R. K.; Luo, S.; Ma, D.; Olsen, J.; Truhlar, D. G.; Gagliardi, L. Multiconfiguration Pair-Density Functional Theory. *Journal of Chemical Theory and Computation* **2014**, *10*, 3669–3680.

(230) Chen, Z.; Zhang, D.; Jin, Y.; Yang, Y.; Su, N. Q.; Yang, W. Multireference Density Functional Theory with Generalized Auxiliary Systems for Ground and Excited States. *J. Phys. Chem. Lett.* **2017**, *8*, 4479–4485.

(231) Peach, M. J. G.; Williamson, M. J.; Tozer, D. J. Influence of Triplet Instabilities in TDDFT. *J. Chem. Theory Comput.* **2011**, *7*, 3578–3585.

(232) Liu, Y.; Li, C.; Ren, Z.; Yan, S.; Bryce, M. R. All-organic thermally activated delayed fluorescence materials for organic light-emitting diodes. *Nat. Rev. Mater.* **2018**, *3*, 18020.

(233) Shang, Q.; Bernstein, E. R. Solvation effects on the electronic structure of 4âĂŘN, NâĂŘdimethylaminobenzonitrile: Mixing of the local $\pi\pi$ and chargeâĂŘtransfer states. *J. Chem. Phys.* **1992**, *97*, 60–68.

(234) Mo, Y.; Gao, J. Polarization and Charge-Transfer Effects in Aqueous Solution via *Ab Initio* QM/MM Simulations. *J. Phys. Chem. B* **2006**, *110*, 2976–2980.

(235) Messina, F.; Bräm, O.; Cannizzo, A.; Chergui, M. Real-time observation of the charge transfer to solvent dynamics. *Nat. Comm.* **2013**, *4*, 2119.

(236) Rondi, A.; Rodriguez, Y.; Feurer, T.; Cannizzo, A. Solvation-Driven Charge Transfer and Localization in Metal Complexes. *Acc. Chem. Res.* **2015**, *48*, 1432–1440.

(237) Sun, H.; Hu, Z.; Zhong, C.; Chen, X.; Sun, Z.; Brédas, J.-L. Impact of Dielectric Constant on the Singlet–Triplet Gap in Thermally Activated Delayed Fluorescence Materials. *J. Phys. Chem. Lett.* **2017**, *8*, 2393–2398.

(238) Sun, H.; Autschbach, J. Electronic Energy Gaps for π-Conjugated Oligomers and Polymers Calculated with Density Functional Theory. *J. Chem. Theory Comput.* **2014**, *10*, 1035–1047.

(239) Egger, D. A.; Weissman, S.; Refaely-Abramson, S.; Sharifzadeh, S.; Dauth, M.; Baer, R.; Kümmel, S.; Neaton, J. B.; Zojer, E.; Kronik, L. Outer-Valence Electron Spectra of Prototypical Aromatic Heterocycles from an Optimally Tuned Range-Separated Hybrid Functional. *J. Chem. Theory Comput.* **2014**, *10*, 1934–1952.

(240) Zhang, C.-R.; Sears, J. S.; Yang, B.; Aziz, S. G.; Coropceanu, V.; Brédas, J.-L. Theoretical Study of the Local and Charge-Transfer Excitations in Model Complexes of Pentacene–C60 Using Tuned Range-Separated Hybrid Functionals. *J. Chem. Theory Comput.* **2014**, *10*, 2379–2388.

(241) Wang, J.; Becke, A. D.; Smith, V. H. Evaluation of $\langle S^2 \rangle$ in restricted, unrestricted Hartree–Fock, and density functional based theories. *J. Chem. Phys.* **1995**, *102*, 3477–3480.

(242) Fuchs, M.; Niquet, Y.-M.; Gonze, X.; Burke, K. Describing static correlation in bond dissociation by Kohn–Sham density functional theory. *J. Chem. Phys.* **2005**, *122*, 094116.

(243) Ess, D. H.; Johnson, E. R.; Hu, X.; Yang, W. Singlet- Triplet Energy Gaps for Diradicals from Fractional-Spin Density-Functional Theory. *J. Phys. Chem. A* **2010**, *115*, 76–83.

(244) Phillips, H.; Geva, E.; Dunietz, B. D. Calculating Off-Site Excitations in Symmetric Donor–Acceptor Systems via Time-Dependent Density Functional Theory with Range-Separated Density Functionals. *J. Chem. Theory Comput.* **2012**, *8*, 2661–2668.

(245) Richard, R. M.; Herbert, J. M. Time-Dependent Density-Functional Description of the ^1L_a State in Polycyclic Aromatic Hydrocarbons: Charge-Transfer Character in Disguise? *J. Chem. Theory Comput.* **2011**, *7*, 1296–1306.

(246) Wong, B. M.; Hsieh, T. H. Optoelectronic and Excitonic Properties of Oligoacenes: Substantial Improvements from Range-Separated Time-Dependent Density Functional Theory. *J. Chem. Theory Comput.* **2010**, *6*, 3704–3712.

(247) Sun, H.; Zhang, S.; Sun, Z. Applicability of optimal functional tuning in density functional calculations of ionization potentials and electron affinities of adenine-thymine nucleobase pairs and clusters. *Phys. Chem. Chem. Phys.* **2015**, *17*, 4337–4345.

(248) Bokareva, O. S.; Möhle, T.; Neubauer, A.; Bokarev, S. I.; Lochbrunner, S.; Kühn, O. Chemical Tuning and Absorption Properties of Iridium Photosensitizers for Photocatalytic Applications. *Inorganics* **2017**, *5*, 23.

(249) Alipour, M.; Fallahzadeh, P. First principles optimally tuned range-separated density functional theory for prediction of phosphorus-hydrogen spin-spin coupling constants. *Phys. Chem. Chem. Phys.* **2016**, *18*, 18431–18440.

(250) Sun, H.; Hu, Z.; Zhong, C.; Zhang, S.; Sun, Z. Quantitative Estimation of Exciton Binding Energy of Polythiophene-Derived Polymers Using Polarizable Continuum Model Tuned Range-Separated Density Functional. *J. Phys. Chem. C* **2016**, *120*, 8048–8055.

(251) Zheng, Z.; Brédas, J.-L.; Coropceanu, V. Description of the Charge Transfer States at the Pentacene/C_{60} Interface: Combining Range-Separated Hybrid Functionals with the Polarizable Continuum Model. *J. Phys. Chem. Lett.* **2016**, *7*, 2616–2621.

(252) Zhuravlev, A. V.; Zakharov, G. A.; Shchegolev, B. F.; Savvateeva-Popova, E. V. Antioxidant Properties of Kynurenines: Density Functional Theory Calculations. *PLoS Comp. Bio.* **2016**, *12*, e1005213.

(253) Bokareva, O. S.; Shibl, M. F.; Al-Marri, M. J.; Pullerits, T.; Kühn, O. Optimized Long-Range Corrected Density Functionals for Electronic and Optical Properties of Bare and Ligated CdSe Quantum Dots. *J. Chem. Theory Comput.* **2017**, *13*, 110–116.

(254) Garza, A. J.; Osman, O. I.; Asiri, A. M.; Scuseria, G. E. Can Gap Tuning Schemes of Long-Range Corrected Hybrid Functionals Improve the Description of Hyperpolarizabilities? *J. Phys. Chem. B* **2015**, *119*, 1202–1212.

(255) Cabral do Couto, P.; Hollas, D.; Slavíček, P. On the Performance of Optimally Tuned Range-Separated Hybrid Functionals for X-ray Absorption Modeling. *J. Chem. Theory Comput.* **2015**, *11*, 3234–3244.

(256) Minami, T.; Ito, S.; Nakano, M. Theoretical Study of Singlet Fission in Oligorylenes. *J. Phys. Chem. Lett.* **2012**, *3*, 2719–2723.

(257) Rangel, T.; Berland, K.; Sharifzadeh, S.; Brown-Altvater, F.; Lee, K.; Hyldgaard, P.; Kronik, L.; Neaton, J. B. Structural and excited-state properties of oligoacene crystals from first principles. *Phys. Rev. B* **2016**, *93*, 115206.

(258) Henderson, T. M.; Janesko, B. G.; Scuseria, G. E. Range Separation and Local Hybridization in Density Functional Theory. *J. Phys. Chem. A* **2008**, *112*, 12530–12542.

(259) Kohn, A. W. Modeling non-radiative processes in solar materials. Ph.D. thesis, Massachusetts Institute of Technology, 2018.

(260) Geva, N. Simulating energy transfer between nanocrystals and organic semiconductors. Ph.D. thesis, Massachusetts Institute of Technology, 2018.

Graphical TOC Entry